frontiers | Frontiers in Marine Science

TYPE Original Research
PUBLISHED 03 October 2024
DOI 10.3389/fmars.2024.1406896

OPEN ACCESS

EDITED BY
Jun Sun,
China University of Geosciences, Wuhan, China

REVIEWED BY
Xiaofan Luo,
Tianjin University, China
Arthur Capet,
Royal Belgian Institute of Natural Sciences, Belgium

*CORRESPONDENCE
Jan Kossack
jan.kossack@hereon.de

RECEIVED 25 March 2024
ACCEPTED 04 September 2024
PUBLISHED 03 October 2024

CITATION
Kossack J, Mathis M, Daewel U, Liu F, Demir KT, Thomas H and Schrum C (2024) Tidal impacts on air-sea CO_2 exchange on the North-West European shelf. *Front. Mar. Sci.* 11:1406896. doi: 10.3389/fmars.2024.1406896

Tidal impacts on air-sea CO_2 exchange on the North-West European shelf

Jan Kossack[1]*, Moritz Mathis[1], Ute Daewel[1], Feifei Liu[1], Kubilay Timur Demir[1], Helmuth Thomas[2,3] and Corinna Schrum[1,4]

[1]Institute of Coastal Systems, Helmholtz-Zentrum Hereon, Geesthacht, Germany, [2]Institute of Carbon Cycles, Helmholtz-Zentrum Hereon, Geesthacht, Germany, [3]Institute for Chemistry and Biology of the Sea, Carl von Ossietzky University Oldenburg, Oldenburg, Germany, [4]Institute of Oceanography, University Hamburg, Hamburg, Germany

Tidal forcing is a dominant physical forcing mechanism on the Northwest European Shelf (NWES) that regulates the mixing-stratification status of the water column and thus acts as a major control for biological productivity and air-sea CO_2 exchange. Tides further influence the marine carbon cycle on the shelf by affecting benthic-pelagic coupling, vertical mixing and the large-scale residual circulation. The cumulative tidal impact on oceanic uptake of atmospheric CO_2 on the NWES, however, remains largely unexplored. We use a coupled physical-biogeochemical ocean model to gain quantitative understanding of the tidal impacts on the air-sea CO_2 exchange of the NWES by comparing hindcast simulations with and without tidal forcing. Our results show that tidal forcing weakens the annual oceanic CO_2 uptake on the NWES by 0.15 $Tmol\ C\ yr^{-1}$, corresponding to a ~13% stronger CO_2 sink in the experiment without tidal forcing. The tide-induced increase in marine primary production demonstrated in earlier studies, which primarily enhances biological carbon fixation in shallow inner-shelf regions of the NWES, does not significantly affect net air-sea CO_2 exchange. Instead, we find tidal mixing, tide-induced baroclinic circulation and the tidal impact on benthic-pelagic coupling to be dominant controls of air-sea CO_2 exchange. Tidal mixing in the permanently mixed shelf regions accounts for the majority (~40%) of the weakening effect on CO_2 uptake, while the modulation of water mass composition in the Celtic Sea by tide-induced baroclinic circulation reduces the uptake further (~33% of the difference in annual mean CO_2 uptake). In terms of the shelf carbon budget, the tidal response of air-sea CO_2 exchange is primarily mediated by changes to the pelagic DIC reservoir (~73%; $-0.11\ Tmol\ C\ yr^{-1}$). Tidal impacts on off-shelf carbon export to the North Atlantic only account for ~20% ($-0.03\ Tmol\ C\ yr^{-1}$) of the tidal impact on shelf CO_2 uptake, and changes in sedimentation of particulate organic carbon account for the remaining ~7% ($-0.01\ Tmol\ C\ yr^{-1}$).

KEYWORDS

NW Europe, tides, internal tides, marine carbon cycle, 3D coupled hydrodynamic-biogeochemical modeling, air-sea CO_2 exchange

1 Introduction

Tidal forcing is one of the dominant physical forcing mechanisms on the Northwest European Shelf (NWES) and affects turbulent mixing, stratification and circulation on the shelf. Being a broad mid-latitude continental shelf, the NWES forms a highly dynamic land-ocean transition zone that connects the terrestrial and ocean carbon reservoirs (Bauer et al., 2013). The continental shelf pump mechanism (Tsunogai et al., 1999), which efficiently exports carbon-enriched subsurface waters from the shelf into the deep North Atlantic, further makes the NWES a vital part of the global ocean carbon sink (Thomas et al., 2004; Legge et al., 2020). Despite its relevance, major knowledge gaps remain regarding the control of oceanic CO_2 uptake on the NWES and the relative contributions of tides and other shelf-specific processes. Therefore, large uncertainties persist regarding the magnitude, variability and future development of carbon sequestration on the NWES (Legge et al., 2020; Ward et al., 2020; Dai et al., 2022).

Tidal forcing affects a wide range of physical and biogeochemical processes that are relevant for the marine carbon cycle on the NWES. Bottom-driven tidal mixing structures the NWES into shallow permanently mixed regions, transitionary regions with tidal fronts and weak stratification and seasonally stratified deep regions (Simpson and Hunter, 1974). Tides can also generate vertical mixing in stratified shelf regions by causing intermittent shear instabilities within the pycnocline (Rippeth, 2005; Becherer et al., 2022). Several studies report elevated pycnocline mixing associated with the internal tide at the shelf break and adjacent outer shelf regions of the NWES (New and Pingree, 1990; Rippeth and Inall, 2002; Sharples et al., 2007). Tides further contribute to the large-scale residual circulation on the NWES by generating baroclinic residual currents (Hill et al., 2008) and also by directly affecting the barotropic residual circulation on the NWES (Tinker et al., 2022). Tides also induce residual mean flow at small-scale bathymetric features, which has been hypothesized to affect the large-scale circulation on the NWES (Polton, 2015).

Tidal forcing has been shown to substantially affect biological productivity on the NWES (Richardson et al., 2000; Sharples, 2008; Zhao et al., 2019; Kossack et al., 2023). Observations further suggest that tidal mixing acts as a major control for air-sea CO_2 exchange on the NWES (Thomas et al., 2004, 2005; Bozec et al., 2006; Prowe et al., 2009). Diapycnal nutrient fluxes induced by internal tides or other tidal processes (Sharples et al., 2007; Becherer et al., 2022) sustain subsurface primary production on the NWES that is suggested to be relevant for air-sea CO_2 exchange (Richardson et al., 2000; Hickman et al., 2012; Rippeth et al., 2014). Tidal impacts on the residual circulation (Hill et al., 2008; Tinker et al., 2022) also affect the large-scale spatial distribution of the carbonate system and thus air-sea CO_2 exchange.

The compound impact of tides on air-sea CO_2 exchange on the NWES is largely unexplored. A fundamental understanding of the role of tidal processes is however relevant for the assessment of potential impacts of climate change on the shelf carbon cycle. Tidal impacts might change over time and with rising sea levels, which will modulate the mixing-stratification status of the tidal shelf system suggested to exert significant control on the magnitude of the continental shelf CO_2 pump (Rippeth et al., 2008). Climate projections further indicate a strengthening of the stratification on the NWES (Holt et al., 2010; Mathis et al., 2018), with potential impacts on internal tides and associated vertical mixing as well as on the density-driven circulation on the NWES (Holt et al., 2022; Tinker et al., 2024). A better understanding of tide-related shelf-specific processes would further provide valuable insights on systematic biases in model-based assessments of the global shelf CO_2 sink, as recently emphasized by Resplandy et al. (2024), as many state-of-the-art global models still do not consider tides.

In this paper, we evaluate tidal impacts on air-sea CO_2 exchange by comparing two separate multi-year numerical model experiments with and without any tidal forcing. We extend the high-resolution coupled physical-biogeochemical regional model framework introduced in Kossack et al. (2023) for the investigation of the marine carbon cycle by incorporating an additional carbonate system model. The model system is based on a flexible unstructured grid that realizes kilometrical-scale horizontal model resolution on the NWES, which for the first time allows an investigation of the impacts of the regionally important internal tide field on air-sea CO_2 exchange in a fully coupled physical-biogeochemical model framework.

We present the details of the applied model configuration, and assess the performance of the carbonate system model in Section 2. In Section 3, we investigate the tidal impacts on air-sea CO_2 exchange and elucidate the role of tidal processes for the shelf carbon cycle. Section 4 discusses the presented results and provides conclusions on the role of tidal forcing for the shelf carbon cycle.

2 Materials and methods

2.1 SCHISM-ECOSMO model configuration

We apply the coupled physical-biogeochemical regional model framework SCHISM-ECOSMO introduced in Kossack et al. (2023) in this study. The 3D hydrodynamic model SCHISM (Zhang et al., 2016) is coupled to the lower trophic level ecosystem model ECOSMO II (Daewel and Schrum, 2013) via the FABM framework (Bruggeman and Bolding, 2014). The additional coupling to a carbonate system model is described in Sect. 2.1.2. We use the high-resolution NWES-IT grid configuration introduced in Kossack et al. (2023). The model domain in NWES-IT extends from 40°N – 66°N and 20° W – 30°E and thus covers the entire NWES as well as a part of the north-east Atlantic (Figure 1). We impose a minimum water depths of 10 m in the model domain. The Baltic Sea is included to adequately resolve basin-exchange processes, but is not particularly attended to in this study, as it does not feature relevant tidal energy.

The physical model component SCHISM is a numerically efficient and robust modelling system based on an unstructured horizontal grid. SCHISM is specifically designed for cross-scale simulation of 3D baroclinic ocean circulation from shallow coastal areas to the deep open ocean (Yu et al., 2017; Ye et al., 2020; Wang et al., 2022). The applied NWES-IT model configuration

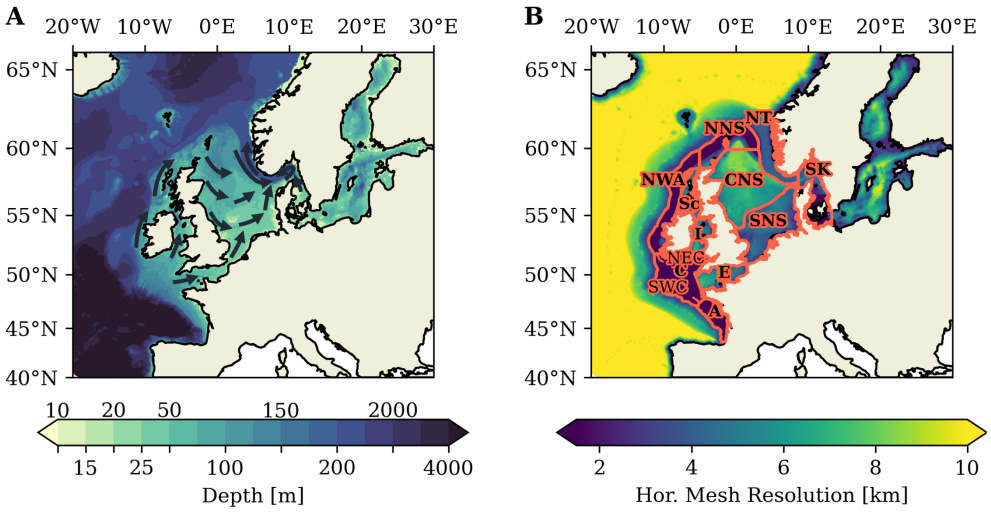

FIGURE 1
Bathymetry in the model domain **(A)**. Arrows schematically show the general circulation on the NWES (adapted from Ricker and Stanev, 2020). Horizontal model resolution of the unstructured triangular grid of the NWES-IT configuration **(B)**. Red lines delineate subareas: southern North Sea (SNS), central North Sea (CNS), northern North Sea (NNS), Skagerrak/Kattegat (SK), Norwegian Trench (NT), N-W Approaches (NWA), Celtic Sea (C), S-W Celtic Sea (SWC), N-E Celtic Sea (NEC), Irish Sea (I), I Sea W. of Sc. (Sc), Armorican shelf (A).

realizes a telescoping high horizontal resolution of 1.5km in the Celtic Sea and in a 75km wide band delimited in off-shelf direction by the 200m isobath. The high-resolution model grid explicitly resolves the kilometrical-scale internal tide field on the NWES (Graham et al., 2018; Guihou et al., 2018; Kossack et al., 2023) and the generation of tide-induced residual mean flow at small-scale bathymetric features (Polton, 2015). The horizontal resolution in the remaining model domain smoothly varies from a maximum of ~ 2.5km in the shallow coastal zones, or even 500m at the Danish Straits, to a minimum resolution of ~ 10km in the deepest parts of the shelf. The horizontal grid resolution in the NWES-IT configuration is shown in Figure 1B. In the vertical, the model applies a flexible Localized Sigma Coordinate with shaved cells (LSC^2) with a maximum of 53 vertical layers. The specific implementation of the physical SCHISM setup and an extensive model validation is provided in Kossack et al. (2023).

The biogeochemical model ECOSMO II uses a nutrient-phytoplankton-zooplankton-detritus (NPZD) conceptual model approach with a total number of 16 state variables (see Figure 2), including three phytoplankton functional groups (diatoms, flagellates and cyanobacteria), two zooplankton functional groups (herbivorous and omnivorous) and three functional groups for detritus (particulate organic matter, dissolved organic matter, biogenic opal). All organic matter pools contain carbon, nitrogen and phosphorous in elemental Redfield ratios of 106:16:1 (Redfield et al., 1963). Benthic-pelagic coupling is implemented as described in Daewel and Schrum (2013). The model considers three different integrated surface sediment pools for each of the three nutrient cycles, one for opal/silicate, one for particulate organic material consisting of carbon, nitrogen and phosphorous at a Redfield ratio, and one for iron-bound phosphorous. Sediment processes include sinking, deposition, and resuspension of particulate organic matter (POM) and opal depending on a critical bottom shear stress, as well as benthic remineralisation of POM and opal. The extended formulation of ECOSMO II allows the simulation of lower trophic level dynamics in a wide range of ecosystems and resolves pelagic and benthic biological processes that affect the marine carbon cycle. The coupled SCHISM-ECOSMO system is introduced and validated by Kossack et al. (2023). The parameter set used here is documented in Supplementary Table S1 in the Supplementary Material.

2.2 Carbonate system model

We employ the FABM framework to further couple the SCHISM-ECOSMO model configuration to the carbonate system model introduced by Blackford and Gilbert (2007). The carbonate system model simulates the carbonate chemistry in seawater based on four state variables: pH, the partial pressure of CO_2 (pCO_2), dissolved inorganic carbon (DIC) and total alkalinity (TA). When two of the four state variables are known, the model estimates the other two iteratively. In the subsequent text, the used model configuration is referred to as SCHISM-ECOSMO-CO2.

Different adaptions of the implemented carbonate system model component have been employed to investigate carbonate chemistry on the NWES in several previous studies (Artioli et al., 2012; Wakelin et al., 2012; Artioli et al., 2014; Blackford et al., 2017). In this study, DIC and TA are provided as prognostic state variables from the ecosystem model component ECOSMO II. The carbonate system model then uses DIC and TA, along with temperature, pressure and salinity, to derive the speciation of DIC in seawater and iteratively solve for pH and pCO_2. The applied carbonate system dissociation constants are taken from Millero et al. (2006).

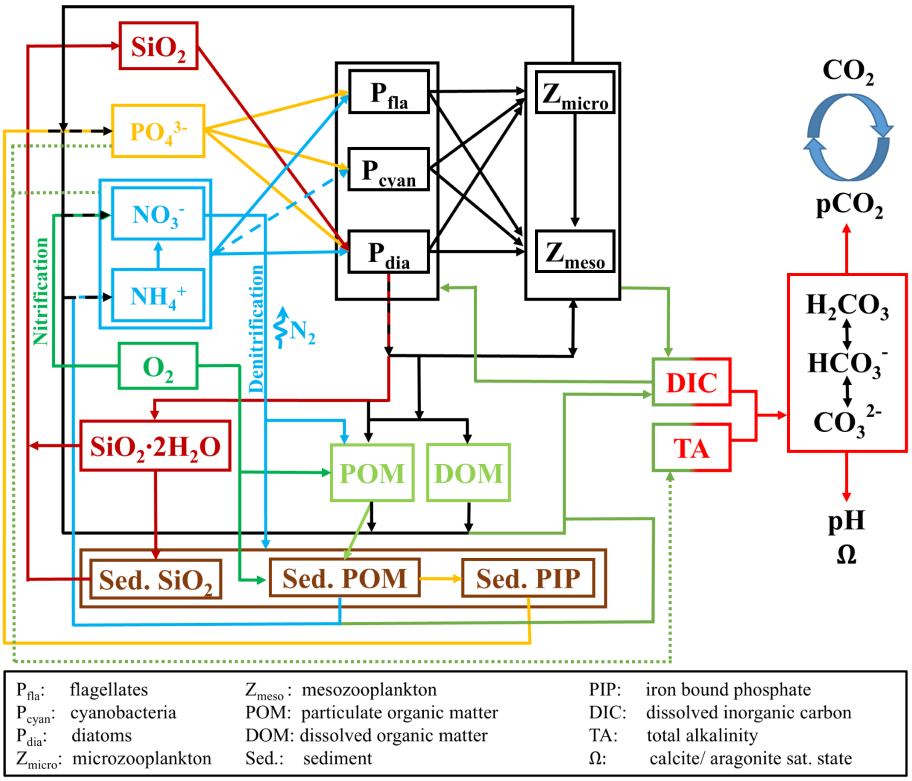

FIGURE 2
Schematic diagram of biochemical interactions in ECOSMO II and coupling to carbonate system model.

Air-sea CO_2 exchange is calculated based on the pCO_2 gradient between the ocean and prescribed atmospheric pCO_2^{air} using the gas transfer parameterization of Wanninkhof (2014).

Figure 2 illustrates the coupling of ECOSMO II and the carbonate system model. Simulated DIC is influenced by organic carbon production by net primary production by the three phytoplankton groups ($NPP_{P1,P2,P3}$), and by organic carbon decomposition by pelagic remineralization of DOM and POM, zooplankton excretion and DIC release from benthic remineralization ($F_{DIC,benthic}$):

$$F_{DIC,\,bio} = \varepsilon_{DOM} C_{DOM} + \varepsilon_{POM} C_{POM} + \mu_1 C_{Z1} + \mu_2 C_{Z2} + F_{DIC,benthic} - NPP_{P1,P2,P3}, \quad (1)$$

Here C_X denotes the respective biomass of DOM, POM, herbivorous zooplankton (Z1) and omnivorous zooplankton (Z2). $\varepsilon_{DOM,\,POM}$ denotes the respective remineralization rates for DOM and POM, and $\mu_{1,2}$ the excretion rates $\mu_{1,2}$ for the two zooplankton groups. We do not simulate a sediment DIC pool and consequently do not include a DIC flux to the sediment. In ECOSMO II, exchange of carbon across the sediment-water interface depends on pelagic-benthic coupling via POM deposition, resuspension and benthic remineralization. Following Daewel and Schrum (2013), pelagic-benthic interaction is defined as:

$$R_{SE} = \lambda_{d2s} C_{POM} - \lambda_{s2d} C_{SE} - \theta(O_2) 2\varepsilon_{SE}(T) C_{SE} - \theta(-O_2)\varepsilon_{SEdenit}(T) C_{SE} - \delta_{bur} C_{SE}$$

Here C_{SE} denotes sediment biomass and δ_{bur} is the loss rate through permanent burial in the sediment. λ_{d2s} is the sedimentation rate if the bottom shear stress is lower than the critical bottom shear stress ($\tau < \tau_{crit} = 0.007\ Nm^{-2}$) and λ_{s2d} is the resuspension rate for $\tau > \tau_{crit}$. The diffusive DIC flux from the sediment into the bottom layer of the water column due to aerobic or anaerobic (denitrification) benthic remineralization is given by:

$$F_{DIC,benthic} = \theta(O_2) 2\varepsilon_{SE}(T) C_{SE} + \theta(-O_2)\varepsilon_{SEdenit}(T) C_{SE},$$

with the temperature-dependent aerobic benthic remineralisation rate $\varepsilon_{SE}(T) = 0.001 e^{0.15T}$ and the denitrification rate $\varepsilon_{SEdenit} = 2\varepsilon_{SE}(T)$.

We implement TA as a fully prognostic variable that is influenced by benthic and pelagic biological processes as described by Wolf-Gladrow et al. (2007) and Gustafsson (2013). TA is explicitly affected by nitrate and ammonium based primary production and aerobic and anaerobic pelagic and benthic remineralization of organic matter in ECOSMO II.

2.3 Model forcing and experiments

Atmospheric forcing and SCHISM-ECOSMO forcing at the open boundaries used in this study are equivalent to Kossack et al. (2023). Boundary conditions for temperature, salinity, nitrate, phosphate, silicate and oxygen are provided from monthly mean WOA2018 climatological data (Boyer et al., 2018) and thus do not include inter-

annual variability. The model configuration used in this study includes spatial varying surface deposition of nitrate and ammonium based on EMEP MSC-W data from MET Norway (https://emep.int/mscw/mscw_moddata.html; downloaded 09/2023), which was not yet implemented in Kossack et al. (2023). Boundary conditions for TA are provided from the global 3D NNGv2LDEO TA climatology (Broullón et al., 2019). Boundary conditions for DIC are provided from the global NNGv2LDEO DIC climatology (Broullón et al., 2020). We add an additional trend for the simulation period derived from a global ICON-coast simulation (Mathis et al., 2022) to account for the effect of rising atmospheric CO_2. Atmospheric pCO_2 is prescribed from monthly mean atmospheric pCO_2 data measured at the Mace Head station (Lan et al., 2022).

River forcing is provided in form of daily river discharge and nutrient, DIC and TA loads for the 172 largest rivers in the domain. River input for ECOSMO state variables other than nutrients are set to zero. River discharge as well as nitrate, ammonium, phosphate and silicate loads represent multi-year daily mean values computed for the period 2000-2015 from a regional river dataset compiled and used by Daewel and Schrum (2013) and further updated by Zhao et al. (2019). We use annual mean concentrations compiled by Pätsch and Lenhart (2008) for riverine DIC, DOM and TA input via the Scheldt, Meuse, Rhine, Ems and Elbe on the European continental coast. We use annual mean concentrations compiled in Neal and Davies (2003) for riverine DIC, DOM and TA input via the Humber estuary, Wear, Twead, Great Ouse and Thames on the eastern UK coast. As done in Kühn et al. (2010), we assume that only 10% of the riverine DOM is bioavailable and, assuming rapid remineralization in the land-ocean transition zone, directly add it to riverine DIC. We prescribe an average DIC concentration of 2700 mmol C m^{-3} computed from Pätsch and Lenhart (2008) for the remaining rivers on the NWES with no available DIC. For missing DOM concentrations, we assume a DOM/DIC ratio of 1/10, of which only 10% is considered bio-available and added to riverine DIC. Due to the overall lack of riverine TA data, we use the end member approach following Hjalmarsson et al. (2008) and Artioli et al. (2012) to estimate riverine TA concentrations for the rivers on the NWES with no available data. For rivers not included in the resulting geographic groupings, we use the average of the estimated riverine TA on the NWES (2050 mmol m^{-3}).

As done in Kossack et al. (2023), a faster coarse resolution SCHISM-ECOSMO-CO2 NWES-LR configuration was used to run a 5 year spin-up simulation from which the initial conditions for the high-resolution configuration used in this study are interpolated. The separate coarser resolution NWES-LR configuration is described in Kossack et al. (2023). Temperature, salinity, nitrate, phosphate, silicate and oxygen for the spin-up simulation were initialized from WOA2018 (Boyer et al., 2018). Initial conditions for DIC and TA are interpolated from the respective NNGv2LDEO climatologies (Broullón et al., 2019, 2020), except for the Baltic Sea, where TA initial conditions are generated using the end-member approach following Hjalmarsson et al. (2008). ECOSMO sediment fields for NWES-LR were interpolated from long-term ECOSMO simulations provided by F. Werner (in pers. comm.) and Samuelsen et al. (2022). Forcing data for the spin-up simulation is equivalent to the high-resolution model configuration described above.

We perform two numerical experiments with the high-resolution SCHISM-ECOSMO-CO2 model configuration to assess the impact of tides on air-sea CO_2 exchange on the NWES. The TIDE experiment includes tidal forcing at the lateral open boundaries and tidal potential in the domain. In the NOTIDE experiment, the same model configuration is run completely without tidal forcing. Both experiments are integrated for a period of 6 years from 2000 to 2005 with hourly instantaneous model output that is averaged to daily means. The first year of the TIDE/NOTIDE experiments is treated as a secondary spin-up period and omitted from the analysis.

2.4 Analysis methods for the carbonate system

2.4.1 Biological and temperature control of pCO_2 in the ocean

We assess the temperature and biological control of surface pCO_2 following the approach proposed by Takahashi et al. (2002), which uses a linearization of the temperature dependency of pCO_2 to differentiate between temperature and biologically driven changes of pCO_2. We calculate the effect of temperature and biology on pCO_2 over an annual cycle as

$$pCO_{2_T} = \overline{pCO_2} \times e^{(0.0423(T-\bar{T}))} \quad (2)$$

$$pCO_{2_{bio}} = pCO_2 \times e^{(0.0423(\bar{T}-T)}, \quad (3)$$

where pCO_2 and T are *in-situ* pCO_2 and temperature, and $\overline{pCO_2}$ and $\bar{T}$ denote annual means. pCO_{2_T} here estimates the pCO_2 values expected from changes in sea surface temperature alone. The biological signal $pCO_{2_{bio}}$ in this approach inherently comprises all non-temperature related effects on pCO_2 (e.g. also changes in TA).

Again, following Takahashi et al. (2002), the ratio of the effects of temperature and biology on surface pCO_2 was calculated to assess the relative importance of biology and temperature over the annual cycle:

$$T/B = \delta pCO_{2_T} / \delta pCO_{2_{bio}}, \quad (4)$$

with the seasonal amplitudes of the change in pCO_2 related to temperature and biological effects:

$$\delta pCO_{2_T} = \max(pCO_{2_T}) - \min(pCO_{2_T}) \quad (5)$$

$$\delta pCO_{2_{bio}} = \max(pCO_{2_{bio}}) - \min(pCO_{2_{bio}}) \quad (6)$$

Regions with annually strong biological effects on pCO_2 will show a smaller T/B ratio, while regions with weaker biological effects on pCO_2 show a higher T/B ratio.

2.4.2 Net community production

We calculate net community production (NCP), i.e. the difference between net primary production and heterotrophic pelagic and benthic remineralization, to evaluate the net change of DIC in the water column evoked by biological processes. We

calculate net community production as

$$NCP = \int_{-H}^{\eta} (NPP_{P1,P2,P3} - HR_P) - F_{DIC,benthic}, \quad (7)$$

where $NPP_{P1,P2,P3}$ is net primary production by the three phytoplankton functional groups, $HR_P = \varepsilon_{DOM} C_{DOM} + \varepsilon_{POM} C_{POM} + \mu_1 C_{Z1} + \mu_2 C_{Z2}$ is pelagic heterotrophic remineralization comprising DOM and POM remineralization and zooplankton excretion (see Equation 1) and $F_{DIC,benthic}$ is the DIC release from benthic remineralization.

2.4.3 Diapycnal fluxes driven by turbulent mixing across the pycnocline

To assess turbulent mixing relevant for the carbonate system, we compute turbulent fluxes of DIC and nitrate following Sharples et al. (2001) and in line with Kossack et al. (2023) as

$$J_{NO3} = -K_V \left(\frac{\Delta NO3}{\Delta z}\right) \quad (8)$$

$$J_{DIC} = -K_V \left(\frac{\Delta DIC}{\Delta z}\right) \quad (9)$$

with the (vertical) eddy diffusivity K_V computed by the model turbulence closure, the difference in nitrate and DIC concentrations between the respective discretized vertical model layers $\Delta NO3$ and ΔDIC, and the vertical model layer thickness Δz in meters. To get the upward diapycnal fluxes from the nutrient-rich deeper water masses into the euphotic zone, we evaluate the diapycnal fluxes at the nutricline z_N (defined as the maximum vertical nitrate gradient in the water column) using daily averaged model output. The nutricline z_N is here assumed to constitute the base of the euphotic zone.

The turbulent nitrate flux J_{NO3} into the euphotic zone can be used to estimate a potential for subsurface primary production, which constitutes a DIC sink that may affect air-sea CO_2 exchange. Assuming full utilization of the vertically mixed nitrate by phytoplankton, we compute potential subsurface primary production as

$$PSP = J_{NO3}(z_N) R_N, \quad (10)$$

where $J_{NO3}(z_N)$ is the turbulent nitrate flux evaluated at the base of the euphotic zone and R_N the standard N:C Redfield ratio.

2.5 Carbonate system model validation

We validate the model results against different observational products to evaluate the model's performance in reproducing the marine carbon cycle on the NWES. We focus on the results of the carbonate system component of the model system. The model performance with respect to general hydrographic conditions and lower trophic level ecosystem dynamics has already been evaluated for the NWES (excluding the Baltic) in Kossack et al. (2023). The subareas used to evaluate model performance in this section (see Figure 1B) are chosen as in Kossack et al. (2023) and account for the spatial heterogeneity of physical and biogeochemical processes on the NWES.

DIC and TA are validated against observational data obtained from the Global Ocean Data Analysis Project version 2 data product (GLODAPv2.2022; Key et al., 2015; Olsen et al., 2016). GODAPv2.2022 comprises a total number of 4283 quality controlled *in situ* seawater samples for DIC and 3824 samples for TA on the NWES in the simulated time period from 2001-2005, the majority of which are from the greater North Sea area. Simulated pCO_2 is validated against observational data obtained from the Surface Ocean CO_2 Atlas version 2023 data product (Sabine et al., 2013; Bakker et al., 2016). SOCATv2023 contains a total number of 786018 *in situ* surface ocean fCO_2 (CO_2 fugacity) measurements collected on the NWES in the simulated time period from 2001-2005. Ocean surface fCO_2 is converted to pCO_2 using the PyCO2SYS v1.8.2 software (Humphreys et al., 2023). The SOCATv2023 data has high temporal and spatial resolutions, but the coverage of the NWES is irregular. Data coverage is high for the greater North Sea region, intermediate in the Celtic Sea and sparse on the North Western Approaches.

2.5.1 DIC and TA validation

We co-locate the observational DIC and TA samples from the GLODAPv2.2022 data product and daily mean model output in time and space for each subarea to quantitatively assess the model's consistency with the spatial and temporal variability of the large-scale carbonate system. Data sparsity limits the quantitative validation of DIC and TA to the greater North Sea area (i.e. the SNS, CNS, NNS, SK and NT subareas in Figure 1B). The direct co-location of observational data and model results is a rigorous test for the model and sensitive to relatively minor spatial and temporal mismatches between model and observations (Allen et al., 2007; Artioli et al., 2012).

Figure 3 shows the normalized and centered statistics of the co-located DIC data for the greater North Sea subareas in form of a Taylor diagram. Correlation coefficients between simulated DIC and observations are > 0.8 for the NNS, NT and SK subareas and 0.79 in the central North Sea. The southern North Sea shows the lowest correlation for DIC (SNS ≈ 0.52). The normalized standard deviation for DIC is below 1 in all evaluated subareas and lowest in the CNS, indicating an underestimation of the amplitude of DIC variability (in time and space) in the model. Normalized centered root mean square differences (CRMSD) calculated for DIC in the subareas are between 0.5 and 1, which suggests a good fit between the model data and observations. The SNS shows the highest normalized CRMSD, which again underlines reduced model performance for DIC in the shallow SNS compared to the deeper North Sea areas.

The Taylor plot in Figure 3 illustrates that TA shows poorer agreement with observations than DIC, particularly in the northern North Sea subarea. The correlation coefficient between simulated TA and observations is moderately high for the NT ($\approx$ 0.77) and SK ($\approx$ 0.71) subareas, and ≈ 0.51 for the SNS. Correlation is however low in the CNS (≈ 0.26) and statistically insignificant in the deep NNS ($R \approx 0.05$ and p-value > 0.3). The normalized

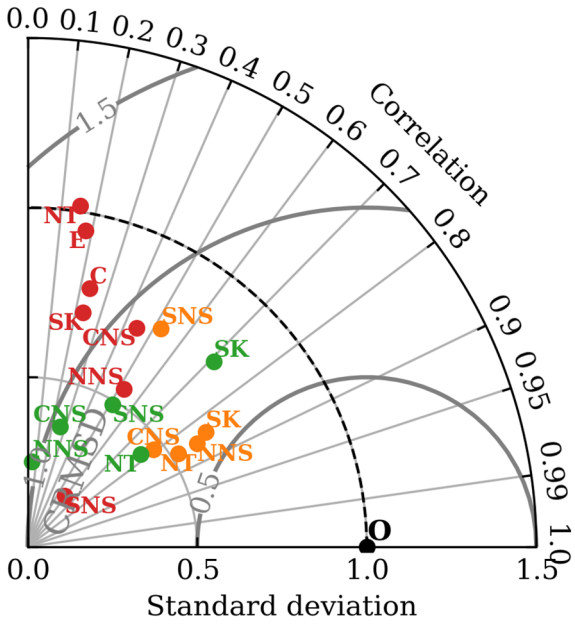

FIGURE 3
Taylor Plot of model DIC data (orange) and TA data (green) co-located against GLODAPv2.2022 data for 2001-2005, and pCO_2 data (red) co-located against SOCATv2023 data for 2001-2005. Statistics are normalized with the standard deviation of the observations. Note that pCO_2 data availability allows the additional evaluation of subareas E and C.

standard deviation for TA is < 0.5 for all subareas except the Skagerrak/Kattegat subarea (NSTD ≈ 0.77), which suggests a general underestimation of the amplitude of TA variability in the model. The normalized standard deviation for TA is particularly low for the CNS (NSTD ≈ 0.37) and the NNS (NSTD ≈ 0.25). Normalized centered root mean square differences for TA are between 0.75 and 1 in the NT, SK, SNS and CNS subareas. The NNS subarea shows the highest normalized CRMSD (> 1).

The evaluation of the percentage bias (i.e. the sum of model error normalized by the data) documented in Table 1 complements the normalized and centered statistics in Figure 3 and provides a measure for systematic over- or underestimation of observations (Allen et al., 2007). The percentage biases for both DIC and TA in Table 1 are ≤ 1 % in all subareas except the SNS, where the percentage bias is 1.7% for DIC and 1.1% for TA. The low percentage bias in Table 1 underlines the good fit between model data and observations demonstrated by the centered statistics in Figure 3, but suggests a minor overestimation of both DIC and TA concentrations in the model. An additional evaluation of the mean bias of seasonal surface DIC concentrations (Supplementary Figure S1 in the Supplementary Material) indicates that the model particularly overestimates surface DIC concentrations in spring (MAM) and summer (JJA). We additionally calculate the cost function (CF) following Holt et al. (2005) as $\chi^2 = \frac{1}{N\sigma_O^2}\sum_{n=1}^{N}(M_n - O_n)^2$, where σ_O is the standard deviation of the observations. The cost function gives a non-dimensional value that indicates the goodness of fit between models and observations. Performance levels are categorized following Radach and Moll (2006) as CF< 1 = very good, 1–2 = good, 2–3 = reasonable, > 3 = poor. The cost function values documented in Table 1 thus suggest very good model performance (CF<1) for DIC in all evaluated subareas except the SNS, which is classified as reasonable. The evaluation of the cost function in Table 1 further corroborates generally reduced model performance for TA. The cost function suggests model performance for TA is highest in the SK and NT subareas (CF<1), good in the SNS and NNS subareas (CF<2) but only poor (CF>3) in the CNS.

2.5.2 pCO_2 validation

The evaluation of surface pCO_2 is an important indicator for the representation of air-sea CO_2 exchange on the NWES, and in combination with the validation of DIC and TA, can provide insights on the main processes responsible for limitations in model performance. Errors in the derived carbonate system variable pCO_2 are larger than in TA and DIC, as errors in DIC, TA and the applied parameterizations accumulate (Artioli et al., 2012; Wakelin et al., 2012). Simulated pCO_2 is quantitatively evaluated by co-locating it in time and space against surface *in situ* measurements obtained from the SOCATv2023 data product for the period 2001-2005. The normalized statistics of the centered co-located pCO_2 data are aggregated for subareas with relevant observational coverage and are shown in the Taylor plot in Figure 3. Table 1 further shows the annual mean percentage bias and the cost function calculated for the co-located pCO_2 data. Simulated mean seasonal pCO_2 for the period 2001-2005 is additionally qualitatively compared against seasonal averages derived from monthly gridded SOCATv2023 observations (Sabine et al., 2013) in Figure 4.

The Taylor plot in Figure 3 shows expected poorer model performance for pCO_2 compared to DIC and TA. The correlations between simulated pCO_2 and SOCATv2023 observations are moderate to low. Correlation is highest for the SNS ($\approx$ 0.59) and the NNS ($\approx$ 0.52). The correlation in the CNS subarea is $\approx$ 0.45, while it is$<$ 0.25 for the remaining SK, NT, E and C subareas. The normalized standard deviation for pCO_2 is$<$ 1 except for the NT subarea (NSTD ≈ 1.02), suggesting a general underestimation of the amplitude of pCO_2 variability in the evaluated subareas of the NWES. The normalized standard deviation is particularly low for the SNS (NSTD ≈ 0.19) subarea. Normalized CRMSD are between 0.5 and 1 for the SNS, CNS and NNS subareas and between 1 and 1.5 for the SK, NT, E and C subareas.

The percentage bias and cost function for pCO_2 shown in Table 1 suggest reasonable model performance in terms of bulk errors. The percentage bias indicates that the model overestimates pCO_2 over the period 2001-2005 in all evaluated subareas except the southern North Sea (Pbias = -13.6%). The percentage bias for pCO_2 is < 5 % in the CNS, NNS and English Channel, and slightly larger than 10% in the SK, NT and Celtic Sea subareas. The cost function calculated for pCO_2 in the respective subareas indicates highest model performance in the North Sea subareas (CF<1), reduced model performance in the SK and E subareas (CF<2) and poorest model performance in the NT and C subareas (CF $\leq$3).

The additional qualitative comparison of simulated seasonal mean pCO_2 to gridded SOCATv2023 data shown in Figure 4

TABLE 1 Statistics from validation of DIC, TA and pCO_2 against observations. DIC/TA model data are co-located in time and space against GLODAPv2.2022 (2001-2005). pCO_2 model data is co-located in time and space against SOCATv2023 (2001-2005).

Subarea	DIC Pbias	DIC CF	TA Pbias	TA CF	pCO_2 Pbias	pCO_2 CF
S. North Sea (SNS)	+1.7%	2.17	+1.1%	1.62	-13.6%	0.86
C. North Sea (CNS)	+1%	0.71	+1%	3.16	+3.7%	0.91
N. North Sea (NNS)	+0.6%	0.5	+0.2%	1.17	+1.3%	0.73
Skag./Kategatt (SK)	+0.5%	0.38	+0.8%	0.82	+13.4%	1.27
Norwegian Trench (NT)	+0.6%	0.46	+0.8%	0.83	+10.4%	2.42
English Channel (E)	–	–	–	–	+4.1%	1.59
Celtic Sea (C)	–	–	–	–	+13.8%	3

The percentage bias is defined following Allen et al. (2007) as $\text{Pbias} = \frac{\sum_{n=1}^{N}(M_n - O_n)}{\sum_{n=1}^{N} O_n} * 100$. The cost function (CF) is defined following Holt et al. (2005) as $\chi^2 = \frac{1}{N\sigma_O^2}\sum_{n=1}^{N}(M_n - O_n)^2$, where σ_O is the standard deviation of the observations.

demonstrates that the model reasonably reproduces the seasonality and spatial variability of surface pCO_2 on the NWES. Figure 4 however also highlights substantial regional differences and temporal variability in the mismatches between simulated pCO_2 and observations.

Simulated mean winter (DJF) pCO_2 compares well against observations in the deeper areas of the North Sea and Celtic Sea. Shallow inner-shelf areas like the English Channel and the southern North Sea in contrast show a strong underestimation of winter pCO_2. The model further moderately underestimates autumn (SON) pCO_2 in parts of the NWES (Figure 4), again particularly in the central and northern North Sea.

The model resolves a strong drawdown of surface pCO_2 in spring induced by biological DIC consumption during the spring bloom, but Figure 4 suggests the model underestimates the magnitude of the spring drawdown in parts of the NWES (i.e. the model overestimates spring pCO_2 compared to the gridded SOCATv2023 data). The overestimation of pCO_2 in spring is particularly high in the shallow southern North Sea, parts of the central North Sea and the Skagerrak. Some shelf regions, for

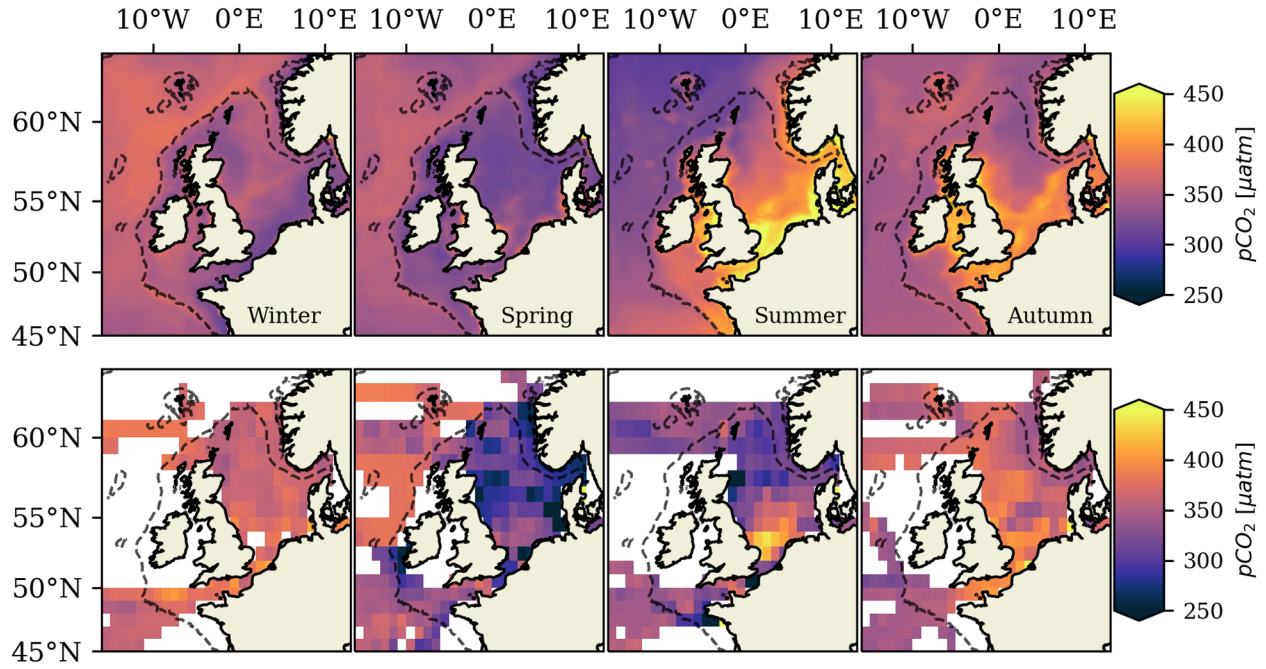

FIGURE 4
Top panel shows simulated seasonal mean surface pCO_2 (2001-2005). Bottom panel shows respective seasonal mean surface pCO_2 obtained from monthly gridded SOCATv2023 observations (Sabine et al., 2013) for the period 2001-2005. The monthly gridded SOCATv2023 observations are binned on a spatial grid of 1° ×1° and constitute cruise weighted averages computed by averaging the arithmetic mean value for each cruise passing through the cell.

example in the English Channel, however, rather locally underestimate mean spring pCO_2. The higher temperature and heterotrophic remineralization of spring bloom remnants increase surface pCO_2 again in summer, especially in permanently mixed shallow inner-shelf regions. The model captures the increase in surface pCO_2, but overestimates summer pCO_2 nearly everywhere on the NWES. The overestimation of summer pCO_2 is particularly high in the Southern Bight region of the North Sea, the Norwegian Trench and parts of the central North Sea. The underestimation of simulated pCO_2 in autumn/winter and the overestimation of spring/summer pCO_2 predominantly identified for central and inner-shelf regions of the NWES cancel out over an annual mean.

2.5.3 Air-sea CO_2 flux validation

We further assess the overall model performance by comparing the simulated annual mean air-sea CO_2 flux in the TIDE experiment (2001-2005) to the observational product of Becker et al. (2021). The simulated air-sea CO_2 flux is additionally evaluated with observation and model-based literature estimates for the NWES. The annual air-sea CO_2 flux in Figure 5A and Table 2 shows that most regions of the NWES are net sinks of CO_2. Simulated oceanic CO_2 uptake is high in deep outer shelf areas and strongest on the N-W Approaches and in the northern North Sea. Simulated oceanic CO_2 uptake is substantially lower or nearly neutral in shallow inner-shelf areas like the southern North Sea and English Channel. Permanently mixed regions in the Irish Sea and along the German North Sea coast show neutral air-sea CO_2 exchange or weak outgassing. The simulated annual CO_2 flux in the Irish Sea suggests the region is a minor source of CO_2 to the atmosphere over the year (see Table 2). ROFIs close to the major rivers on the continental and UK coasts also show outgassing of CO_2 to the atmosphere.

The decrease of the oceanic CO_2 sink from the deep northern North Sea to the shallow southern North Sea qualitatively fits to the spatial structure of observations by Thomas et al. (2004) and the mean air-sea CO_2 flux map for 2001-2005 shown in Figure 5B derived from the data used in Becker et al. (2021). The model shows an increase in CO_2 uptake towards the Fair Isle Channel in

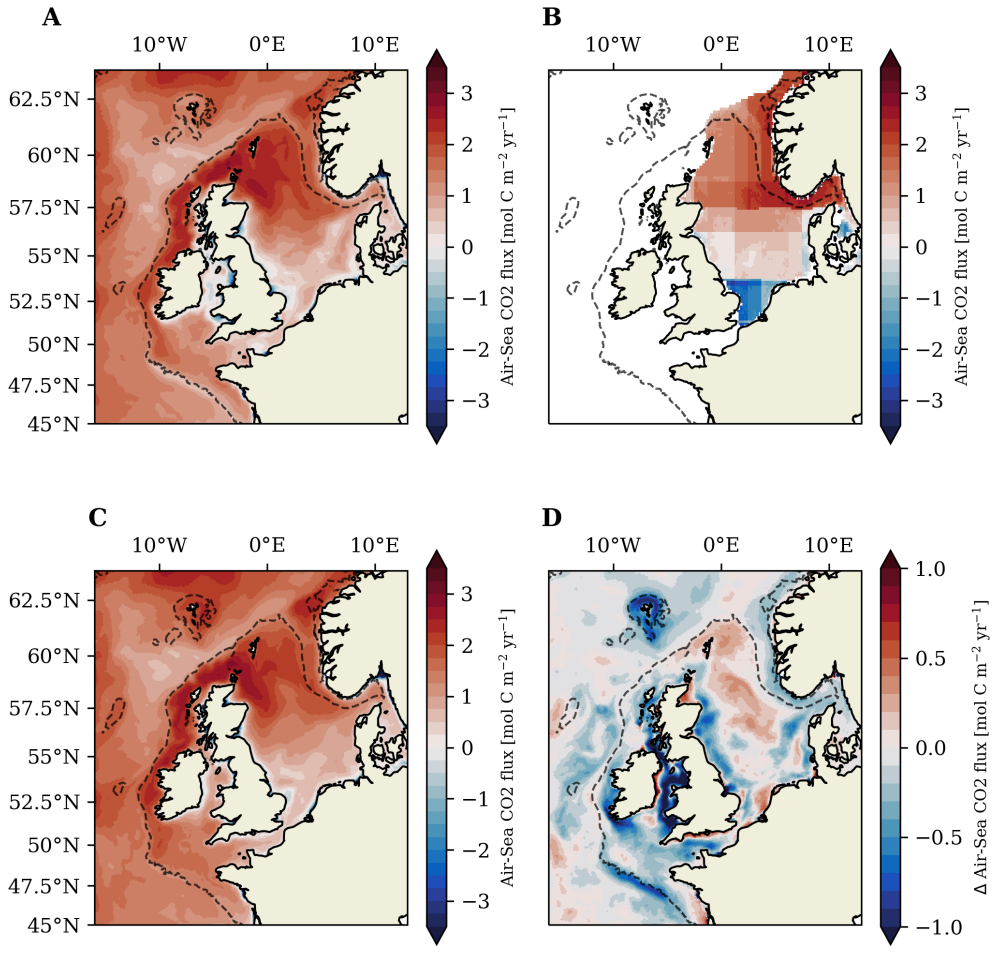

FIGURE 5
Annual mean air-sea CO_2 flux (2001-2005) for TIDE experiment **(A)**. **(B)** shows the mean air-sea CO_2 flux map for 2001-2005 obtained from the data supplement (https://doi.org/10.18160/939X-PMHU, last accessed 06/2024) to Becker et al. (2021). The air-sea flux in Becker et al. (2021) is calculated based on SOCATv5 data using multi linear regression. **(C)** shows the annual mean air-sea CO_2 flux (2001-2005) for the NOTIDE experiment and **(D)** the difference (TIDE – NOTIDE) of the air-sea CO_2 flux between the two experiments. Positive (red) values in **(A–C)** indicate oceanic CO_2 uptake, negative values (blue) indicate outgassing to the atmosphere.

10.3389/fmars.2024.1406896

TABLE 2 Area mean annual CO_2 flux (2001-2005) on the NWES in TIDE and NOTIDE experiments.

	TIDE CO_2 Flux	NOTIDE CO_2 Flux	Δ CO_2 Flux	Δ NCP
Subarea	**Total [Gmol C yr^{-1}] (Mean [mol C m^2yr^{-1}])**	**Total [Gmol C yr^{-1}] (Mean [mol C m^2yr^{-1}])**	**[Gmol C yr^{-1}] (TIDE-NOTIDE)/TIDE**	**[Gmol C yr^{-1}] (TIDE-NOTIDE)/TIDE**
S. North Sea (SNS)	84.4 (0.4)	99.1 (0.5)	-14.6 (-17%)	-24.8 (-24%)
C. North Sea (CNS)	366 (1.5)	366.5 (1.5)	-0.5 (<-1%)	-0.9 (-2%)
N. North Sea (NNS)	165.9 (2.1)	157.6 (2)	8.3 (+5%)	4.4 (+13%)
Skag./Kattegat (SK)	-36 (-0.5)	-30.4 (-0.4)	-5.7 (-16%)	-23 (-23%)
Norwegian Tr. (NT)	101.6 (1.3)	113.7 (1.5)	-12.1 (-12%)	-32.8 (-22%)
English Channel (EC)	37.8 (0.5)	50.8 (0.6)	-13 (-34%)	7.5 (+53%)
Celtic Sea (C)	211.4 (1.07)	265.1 (1.3)	-53.7 (-25%)	-5.6 (-10%)
Irish Sea (I)	-15.4 (-0.3)	8.7 (0.2)	-24.2 (-157%)	6.5 (+28%)
I. Sea W. of Scotl. (Sc)	27.4 (0.6)	39 (0.9)	-11.6 (-43%)	23.1 (+122%)
West Irish Shelf (WI)	73.6 (1.6)	85.4 (1.8)	-11.7 (-16%)	-1.4 (-5%)
Malin Shelf (MS)	44.5 (2.1)	46.7 (2.2)	-2.2 (-5%)	3.3 (+51%)
Hebrides Shelf (HS)	72.4 (2.1)	76.7 (2.2)	-4.3 (-6%)	-0.1 (-1%)
Sum for NWES	1.16 ± 0.08 $Tmol\ C\ yr^{-1}$	1.31 ± 0.11 $Tmol\ C\ yr^{-1}$	-0.15 $TmolC\ yr^{-1}$(-13%)	-0.04 $TmolC\ yr^{-1}$(-7%)

Positive values denote oceanic uptake. Net community production calculated using Equation 7. Differences between the experiments calculated as TIDE-NOTIDE. Proportional differences between experiments are computed relative to TIDE experiment.

the north-east of the North Sea, in agreement with Thomas et al. (2004). Based on an extensive observational campaign in 2001, Thomas et al. (2004) estimate annual oceanic CO_2 uptake of 1.5 – 2.5 $mol\ C\ m^{-2}yr^{-1}$ in the northern North Sea, which compares well to the estimated annual mean flux of 2.1 $mol\ C\ m^{-2}yr^{-1}$ in our simulations. Comparison to Figure 5B suggests the model underestimates annual mean CO_2 uptake in the Norwegian Trench. Our model shows a weak oceanic CO_2 sink in the Southern Bight of the North Sea and the eastern English Channel. Thomas et al. (2004) and Becker et al. (2021) in contrast found the region to be a weak source of CO_2 to the atmosphere (see Figure 5B). Yet there is large interannual variability in the region and studies from different years and with different methodologies conflict in the direction of the CO_2 flux in the region (Thomas et al., 2004; Schiettecatte et al., 2007; Omar et al., 2010; Kitidis et al., 2019).

Simulated annual mean oceanic CO_2 uptake of 0.8 $mol\ C\ m^{-2}yr^{-1}$ in the north-eastern Celtic Sea and 1.4 $mol\ C\ m^{-2}yr^{-1}$ in the south-western Celtic Sea are higher than respective estimates in Marrec et al. (2015), who proposed 0.6 $mol\ C\ m^{-2}yr^{-1}$ for the north-eastern Celtic Sea and 0.9 $mol\ C\ m^{-2}yr^{-1}$ for the south-western Celtic Sea. Frankignoulle and Borges (2001) however estimated a higher oceanic CO_2 uptake of 1.7 – 2.9 $molC\ m^{-2}yr^{-1}$ for the Celtic Sea and Bay of Biscay region. Simulated area-mean weak outgassing of – 0.3 $mol\ C\ m^{-2}yr^{-1}$ in the Irish Sea matches the estimate of – 0.3 $molC\ m^{-2}yr^{-1}$ in Marrec et al. (2015).

The overall mean annual oceanic CO_2 uptake on the NWES (delineated by the 200m isobath plus the Norwegian Trench) for the period 2001-2005 is $1.16 Tmol\ yr^{-1}$, compared to the estimated range of 1.3 – 3.3 $Tmol\ yr^{-1}$ proposed in Legge et al. (2020) based on two observational and two modelling studies. The standard deviation of the simulated annual mean shelf CO_2 uptake, i.e. the interannual variability for the simulation period 2001-2005, is ± 0.08 $Tmol\ yr^{-1}$. The overall mean net annual oceanic CO_2 uptake in the North Sea (here defined as the SNS, CNS and NT subareas) is 0.55 $Tmol\ C\ yr^{-1}$ in our simulations, with a standard deviation of ± 0.03 $Tmol\ C\ yr^{-1}$. Using a slightly larger geographical definition of the North Sea, Thomas et al. (2005a) estimated an annual oceanic CO_2 uptake of 0.794 $Tmol\ yr^{-1}$ for the North Sea based on observational surveys in 2001 and 2002, with an estimated range of uncertainty of 20-50% related to differences in gas transfer parameterizations (Watson et al., 2009; Meyer et al., 2018).

2.6 Validation summary

The validation demonstrates that the applied SCHISM-ECOSMO-CO2 model system reproduces key features of the marine carbon cycle on the NWES. Simulated oceanic CO_2 uptake on the NWES compares favourably with estimates from literature, but the model shows a tendency to underestimate the shelf CO_2 sink. The validation of the carbonate system model state variables DIC and TA indicate quantitative agreement between the model and observational data. Model performance for DIC is better than for TA. The model biases for both DIC and TA indicate a minor overestimation against observations in both variables. Bulk errors for the derived carbonate system model variable pCO_2 suggest reasonable model performance (Table 1), but are larger than for DIC and TA. Further comparison against pCO_2 observations (Figures 3, 4) identifies model limitations in the simulation of the full spatial heterogeneity and temporal variability of the shelf carbonate system.The presented model validation here generally aligns with the modelling studies by

Artioli et al. (2012) and Wakelin et al. (2012), who find comparable quantitative agreement to observations for DIC and TA, and also poorer model performance for pCO_2.

The good quantitative validation results for DIC underline the model's general ability to reproduce the spatial and temporal variability of DIC on the shelf. Model performance for DIC is lower for the shallow and highly heterogenous southern North Sea (SNS) compared to the deeper North Sea areas. The validation suggests that the model underestimates DIC drawdown during the productive season, especially in summer. Overestimated DIC is likely a dominant factor for the identified overestimation of surface pCO_2 in spring and summer (Figure 4), and therefore potentially contributes to the underestimation of the NWES CO_2 sink in the model. The overestimation of DIC in spring and summer is presumably linked to an underestimation of primary productivity commonly identified for ECOSMO II (Daewel and Schrum, 2013; Zhao et al., 2019). Small summer SST warm biases (Kossack et al., 2023) might also locally contribute to the overestimation of surface pCO_2. The strict application of Redfield stoichiometry in ECOSMO II likely is a key factor that contributes to DIC overestimation in the model. Non-Redfield DIC fixation has been observed on the NWES (Bozec et al., 2006; Humphreys et al., 2019), and ecosystem models assuming Redfield stoichiometry in the production and decomposition of organic matter generally tend to underestimate biological carbon fixation, especially in summer (Prowe et al., 2009; Kühn et al., 2010). The introduction of variable stoichiometry is further suggested to improve the seasonality of surface pCO_2 and associated air-sea CO_2 fluxes by reducing the overestimation of surface pCO_2 in summer and the underestimation of surface pCO_2 in autumn and winter (K. Demir, in pers. comm.).

Further model limitations arise from applied model parameterizations. POM is parameterized with a constant sinking rate. POM and DOM remineralization in ECOSMO II are parameterized with only temperature-dependent bulk remineralization rates that potentially contribute to the misrepresentation of spatial and temporal variability of the shelf carbonate system. Further differentiation of size and lability of the POM and DOM compartments, or the explicit parameterization of the microbial loop (Azam et al., 1983) hold potential for further model improvement. Uncertainty in benthic carbon stocks and parameterizations of benthic-pelagic coupling also restrict model performance on the NWES (Legge et al., 2020). Benthic-pelagic coupling is particularly relevant in shelf settings where the sediment and atmosphere can directly interact. Recent work has shown the importance of macrobenthos and associated bioturbation for the sedimentary organic carbon budget and benthic-pelagic coupling (Zhang et al., 2019). The inclusion of macrobenthos and associated bioturbation could potentially improve the seasonal cycle of pelagic DIC concentrations (and associated air-sea CO_2 fluxes) by modulating benthic remineralization and resuspension.

Given the substantial inter-annual variability of DIC concentrations in the eastern North Atlantic (Thomas et al., 2008), the climatological forcing applied at the open boundary further impedes model performance on the NWES. The river loads for DIC and TA also lack seasonal and inter-annual variability. Given the general sparsity of adequate data for riverine and other coastal carbon inputs, the applied riverine forcing is generally subject to particularly high uncertainty (Legge et al., 2020) that limits model performance in the coastal regime. This likely contributes to the lower model performance found for DIC in the southern North Sea.

The use of climatological data at the open boundary also likely limits model performance for TA and potentially contributes to the low TA model skill in the northern North Sea. In contrast to other approaches, the applied prognostic TA model enables the simulation of the highly heterogeneous NWES including the Baltic Sea, for which no single reliable TA-salinity regression is applicable. The complex biological dynamics and coastal processes and inputs that affect TA however are a challenge for the fully prognostic simulation of TA. Benthic processes and associated TA fluxes have been shown to be relevant on the NWES (Brenner et al., 2016), but are only partially reproduced in the model system. Simulated TA will also be restricted by errors in the simulation of nutrient sources and sinks in ECOSMO II (Kossack et al., 2023). Another significant caveat is the large uncertainty in riverine inputs of TA and the lack of adequate (basin-scale) data for additional coastal TA inputs, for example from the Wadden Sea (Thomas et al., 2009). The moderate model performance in the southern North Sea is therefore already promising. The comparatively high model performance in the Skagerrak/Kattegat and the Norwegian Trench further suggests a reasonable representation of TA in the Baltic Sea outflow.

The dynamic shelf environment and the complexity of coastal ecosystems, as well as the large uncertainty in riverine and other coastal inputs relevant to the carbonate system (Legge et al., 2020), make modelling the coastal and shelf carbon cycle very challenging. Despite its limitations, the presented SCHISM-ECOSMO-CO2 model system is accepted to reproduce key features of the marine carbon cycle on the NWES both qualitatively and with reasonable quantitative skill. The moderate complexity of the biogeochemical components of the applied model configuration further facilitates the use of a high horizontal model resolution of 1.5km required to resolve key tidal processes on the NWES (Polton, 2015; Guihou et al., 2018) at reasonable computational cost (Kossack et al., 2023). The model validation therefore encourages the use of SCHISM-ECOSMO-CO2 for the investigation of tidal impacts on the air-sea CO_2 flux in the following sections of the study.

3 Results

3.1 Tidal impacts on air-sea CO_2 exchange

We find that annual mean oceanic CO_2 uptake on the NWES (area delimited by the 200m isobath, excluding the Baltic Sea) is $-0.15\ Tmol\ C\ yr^{-1}$ lower in the experiment with tidal forcing than in the experiment without tidal forcing (Table 2). This amounts to a 13% higher annual mean oceanic CO_2 uptake on the NWES in the NOTIDE experiment (Figure 5C) compared to the TIDE experiment (Figure 5A).

The difference of mean annual air-sea CO_2 flux (2001-2005) between the two experiments documented in Figure 5D and Table 2

shows spatially heterogeneous tidal impacts on the air-sea CO_2 flux on the NWES. Tidal forcing substantially decreases oceanic CO_2 uptake in large parts of the NWES, predominantly in shallow inner-shelf regions. The relative difference in the air-sea CO_2 exchange is particularly pronounced in the Irish Sea (-157%), which shows net CO_2 outgassing over the annual cycle in the TIDE experiment but net oceanic CO_2 uptake in the NOTIDE experiment. Inner-shelf subareas like the North-Eastern Celtic Sea (-44%) or the English Channel (-34%) also show a relevant reduction of oceanic CO_2 uptake. Tidal forcing however also increases oceanic CO_2 uptake (up to 1 $molC\ m^{-2}yr^{-1}$), predominantly in seasonally stratified areas in the central and northern North Sea. The northern North Sea is the only subarea in which tidal forcing marginally increases mean annual oceanic CO_2 uptake (+5%). The seasonally stratified Celtic Sea in contrast shows a distinct reduction of mean annual oceanic CO_2 uptake. The tidal impacts on the air-sea CO_2 flux on the outer-shelf N-W Approaches are generally negligible, with only small local decreases of oceanic CO_2 uptake in shallow near-coast areas. Figure 5D however indicates that tidal forcing substantially decreases oceanic CO_2 uptake on the continental slope along the Celtic Sea and on adjacent outer-shelf areas of the south-western Celtic Sea.

3.2 Understanding the mechanisms behind the tidal impacts on air-sea CO_2 exchange

3.2.1 Tidal impacts on the NWES carbon budget

The strongest tidal imprints on the net carbon budget are found in the carbon enrichment of the shelf waters and the net carbon transfer to the sediments. Tide-induced processes decrease the total pelagic DIC stock (~240.5 Tmol C in the TIDE experiment and ~240.9 Tmol C in the NOTIDE experiment for 2001-2005), as neglecting tides results in a ~50% stronger DIC enrichment of 0.34 Tmol C yr^{-1}, compared to an accumulation rate of 0.23 Tmol C yr^{-1} when tides are included. Net carbon sedimentation on the NWES is low in the TIDE experiment (0.001 Tmol C yr^{-1}; mean for 2001-2005). Neglecting tides, and therefore primarily the impact of physical resuspension, considerably increases POC deposition and results in an elevated sediment carbon content (Figure 6). Although benthic remineralization returns the bulk of the carbon in the sediments back to the water column in the NOTIDE experiment, the resulting net sedimentation rate is higher by a factor of 10 (0.01 Tmol C yr^{-1}). Prescribed riverine carbon input is the same in both experiments (2.04 Tmol C yr^{-1}) and the net carbon import from the Baltic Sea is only marginally affected by tidal forcing (0.45 Tmol C yr^{-1} in the TIDE and 0.41 Tmol C yr^{-1} in the NOTIDE experiment). By closing the carbon budget, we infer that ~0.93 Tmol C yr^{-1} (or ~80%) of the annual shelf CO_2 uptake in the TIDE experiment (1.16 Tmol C yr^{-1}) is exported off-shelf, while ~0.96 Tmol C yr^{-1} (or ~73%) of the annual CO_2 uptake (1.31 Tmol C yr^{-1}) is exported off-shelf in the NOTIDE experiment.

3.2.2 Tidal impacts on net community production

Tidal forcing has been shown to substantially increase net primary production (NPP) on the NWES (Kossack et al., 2023). Changes in heterotrophic remineralization however also need to be considered to obtain the net tidal impact on biological carbon cycling on the NWES. We directly evaluate tidal impacts on net community production (i.e. the metabolic balance between NPP and heterotrophic remineralization) computed with Equation 7 to assess tidal impacts on biological cycling of carbon. Mean annual NCP in the TIDE and NOTIDE experiments is shown in Figures 7A, B, respectively. The difference in mean annual NCP between the TIDE and NOTIDE experiments is shown in Figure 7C and additionally documented in Table 2.

Our results suggest that the entire NWES is net heterotrophic ($NCP = -0.62\ Tmol\ C\ yr^{-1}$) in the TIDE experiment (mean for 2001-2005). The North Sea is also net heterotrophic ($NCP = -0.32\ Tmol\ C\ yr^{-1}$) in the TIDE experiment, with particularly negative NCP (i.e. strong heterotrophy) in the Norwegian Trench. Figure 7C and Table 2 show a spatially heterogeneous tidal response of NCP on the NWES, and suggest that tides make the NWES slightly more heterotrophic (by $-0.04\ Tmol\ C\ yr^{-1}$). The difference between the experiments amounts to ~7% (relative to the TIDE experiment). Including tides decreases the burial of POC in the sediment by $\sim 0.009\ Tmol\ C\ yr^{-1}$ (see Sect. 3.2.1). This decrease in the net removal of organic carbon from the NWES carbon cycle explains about ¼ of the increase in heterotrophy (i.e. decrease in NCP) with tidal forcing. As other organic carbon fluxes on the NWES are not changed in the sensitivity experiment without tidal forcing, the remaining increase in heterotrophy with tidal forcing implies higher organic carbon import onto the NWES. We therefore find that although tides substantially increase net primary production on the NWES, this does not move the shelf system closer to autotrophy.

The tidal impact on heterotrophic remineralization is primarily facilitated through the strong tidal impact on benthic-pelagic coupling on the shelf (see Sect. 3.2.1). Higher sedimentation of POC in the NOTIDE experiment redistributes heterotrophic remineralization from the water column into the sediment. Benthic heterotrophic remineralization is also slower than pelagic heterotrophic remineralization (Krumins et al., 2013). The difference in the parameterized remineralization rates (see parameter set in Supplementary Table S1 in the Supplementary Material) therefore additionally affects the timing of heterotrophic remineralization in the two experiments. Heterotrophic remineralization in the TIDE experiment consequently occurs earlier in the annual cycle than in the NOTIDE experiment. Compared to the TIDE experiment, the NOTIDE experiment is more autotrophic in summer and more heterotrophic in autumn and winter (see Supplementary Figure S2 in the Supplementary Material).

Tidal impacts on mean annual NCP in Figure 7C show large spatial heterogeneity on the NWES. Tidal impacts on NCP are most pronounced in inner-shelf regions, where Figure 7C shows areas with strong increases of NCP with tidal forcing, but often also directly adjacent areas of strong decreases of NCP. Tidal impacts on NCP in the deeper shelf regions are generally smaller, but also show a pattern of local increases and local decreases. Only the northern North Sea shows a moderate net increase in NCP with tidal forcing (Table 2), particularly in the region east of the Shetland Islands. The observed spatial pattern in the tidal response of NCP in Figure 7C,

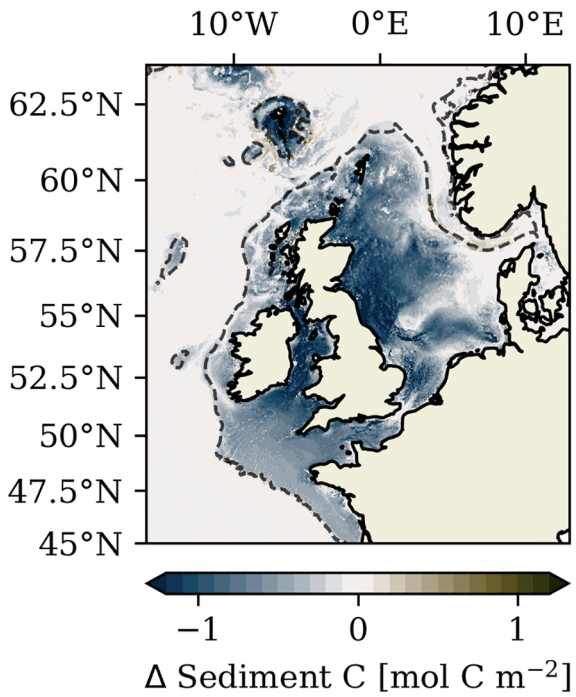

FIGURE 6
Difference of the annual mean sediment organic carbon inventories (2001-2005) between the two experiments (TIDE-NOTIDE).

with local increases and often adjacent local decreases of NCP, is consistent with the strong tidal impact on benthic-pelagic coupling and suggest advective transport of tidally resuspended POM. The tidally resuspended POM is advected downstream, for example with the cyclonic circulation in the North Sea (see Figure 1A), while the sedimented POM in the NOTIDE experiment remains stationary. Advective transport of POM out of a specific area decreases local heterotrophic remineralization relative to primary production, i.e. it increases local autotrophy. Local increases in heterotrophy in turn suggests tides enhance advective transport of organic matter into

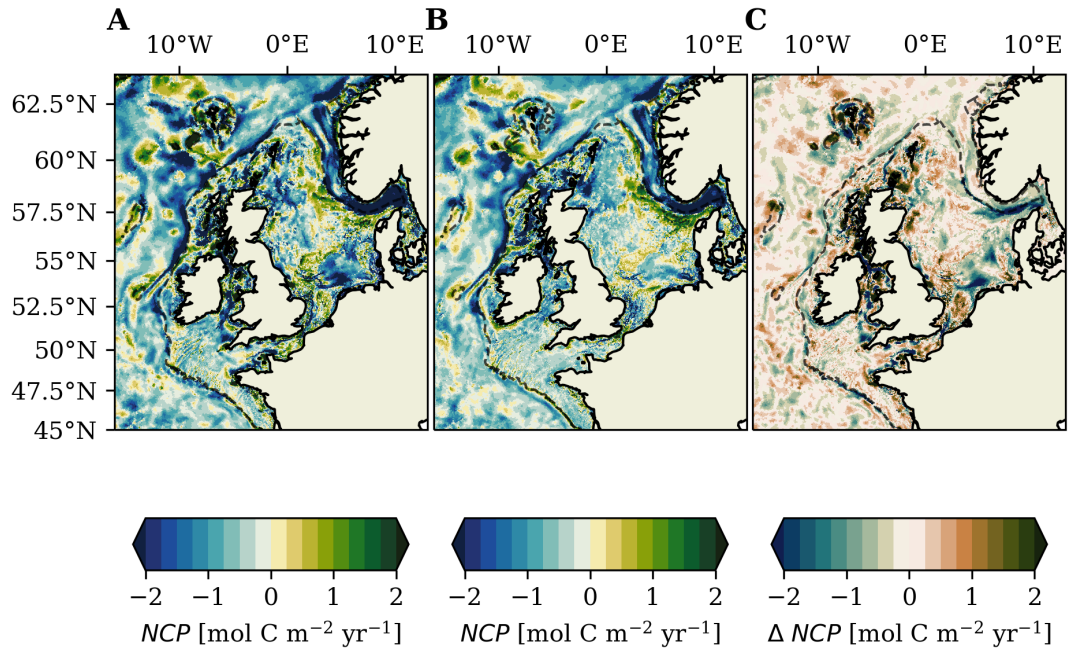

FIGURE 7
Mean annual net community production (2001-2005; Equation 7) in **(A)** TIDE experiment and **(B)** NOTIDE experiment. **(C)** Difference of mean annual net community production (2001-2005) in the two experiments (TIDE – NOTIDE).

the respective area. The substantial reduction of NCP with tidal forcing in the Norwegian Trench ($-32.8\ Gmol\ C\ yr^{-1}$) suggests tides are particularly important for organic matter transport from the North Sea shelf into the Norwegian Trench.

Tidal forcing therefore mainly laterally redistributes organic matter on the shelf, affects the balance of benthic and pelagic heterotrophic remineralization and determines the timing of heterotrophic remineralization. The large mismatches between the tidal impacts on the air-sea CO_2 flux and tidal impacts on NCP shown in Table 2 however suggests there is no direct relationship between the tidal impacts on NCP and air-sea CO_2 exchange. The discrepancies are particularly large in shallow inner-shelf regions like the Irish Sea and English Channel, where tides decrease annual mean oceanic CO_2 uptake even though tidal forcing makes the subareas more autotrophic (which generally facilitates more CO_2 uptake from the atmosphere). This indicates that other tidal processes are the prevailing factor for the tidal impacts on air-sea CO_2 flux in shallow inner-shelf regions.

3.2.3 Tidal impacts in permanently mixed regions

Tidal mixing partitions the shelf into permanently mixed and seasonally stratified regions, which both constitute distinct biogeochemical regimes with implications for air-sea CO_2 exchange (Thomas et al., 2004). Seasonal stratification enables the drawdown of surface DIC concentrations by means of the biological pump mechanism (Volk and Hoffert, 1985). The drawdown of surface DIC in spring and summer counteracts the effect of seasonal warming, which drives up surface pCO_2, and thus facilitates net oceanic uptake of atmospheric CO_2 over the annual cycle. In permanently mixed regions, primary production and heterotrophic remineralization are not vertically separated and (respired) carbon in the water column can constantly exchange with the atmosphere. Strong tidal resuspension of POM from the sediment additionally increases the organic carbon pool available for pelagic heterotrophic remineralization in spring and summer. Permanently mixed regions consequently generally exhibit weak air-sea CO_2 exchange or show a tendency to weak outgassing of excess carbon to the atmosphere (i.e. from riverine input).

Neglecting tides leads to a larger part of the shallow inner-shelf being seasonally stratified (see Supplementary Figure S3 in the Supplementary Material), which in turn affects biogeochemical cycling in the region. We investigate the associated tidal impact on air-sea CO_2 exchange by evaluating the tidal impacts on temperature and biological control of surface pCO_2. We use Equations 2, 3 to calculate the effects of temperature and biology on pCO_2 from monthly mean surface pCO_2 and SST (2001-2005). We subsequently use Equations 5, 6 to compute δpCO_{2_T} and $\delta pCO_{2_{bio}}$, the respective mean seasonal amplitudes of surface pCO_2 changes related to temperature and biology, and assess the relative importance of temperature and biological effects on pCO_2 over the mean annual cycle by means of the T/B ratio calculated with Equation 4.

The T/B ratio in the TIDE experiment (Figure 8A) shows that the temperature effect on surface pCO_2 strongly dominates in inner-shelf areas, while central and outer shelf areas exhibit a stronger biological effect on pCO_2. The tidal impact on the T/B ratio shown in Figure 8B, i.e. the difference between the T/B ratio in the TIDE and NOTIDE experiments, demonstrates that tidal forcing is largely responsible for the relative dominance of the temperature effect on surface pCO_2 in the areas that are permanently mixed in the TIDE experiment. The tidal impact on the T/B ratio in central and outer shelf regions is generally low.

In general, tides affect both temperature and biological control on pCO_2, which in turn determines the tidal impact on the T/B ratio. Tidal mixing affects temperature control of pCO_2 by modulating oceanic heat uptake on the NWES (Arnold et al., 2021), which results in colder summer SST and warmer winter SST in the shallow inner-shelf areas of the NWES (Supplementary Figure S4 in the Supplementary Material). Neglecting tides thus results in a larger seasonal amplitude of the temperature effect on pCO_2 (δpCO_{2_T}; Equation 5) on most of the NWES (Figure 8C), which suggests larger temperature control on air-sea CO_2 exchange in the NOTIDE experiment. The tidal impact on δpCO_{2_T} is however small compared to the tidal impact on the biological effect on pCO_2 ($\delta pCO_{2_{bio}}$; Equation 6) shown in Figure 8D. Neglecting tides results in a larger seasonal amplitude of pCO_2 changes related to biology (i.e. a stronger biological control of pCO_2) on the NWES, particularly in regions that are permanently mixed regions in the TIDE experiment, but are seasonally stratified in the NOTIDE experiment (Supplementary Figure S3 in the Supplementary Material). Our results therefore indicate that it is mainly the tidal weakening of the biological effect on pCO_2 that causes the tidal impact on the T/B ratio documented Figure 8B.

Figure 8E exemplifies the tidal impact on surface pCO_2 at a station in the permanently mixed Irish Sea. The strong tidal mixing in the Irish Sea nearly completely offsets the biological buffering of the temperature-driven pCO_2 increase during seasonal warming, and thus leads to temperature-driven net outgassing in the Irish Sea over the annual cycle (Table 2). If tides are neglected, the water column at the station is seasonally stratified and allows the biological buffering of the seasonal warming effect, which draws down surface pCO_2 in summer and enables net oceanic CO_2 uptake in the Irish Sea over the annual cycle.

The analysis of the tidal impact on the T/B ratio demonstrates how the partitioning of the NWES into seasonally stratified and permanently mixed regions plays a key role in controlling surface pCO_2, and thus air-sea CO_2 exchange. Dominance of temperature control on pCO_2 in the permanently mixed shelf regions ultimately entails stronger CO_2 outgassing in summer (Thomas et al., 2004), which limits annual CO_2 uptake or even leads to net outgassing like in the Irish Sea. We find that the permanently mixed regions (as defined in Figure 8B) alone account for ~40% ($-0.06\ Tmol\ C\ yr^{-1}$) of the difference in oceanic CO_2 uptake on the NWES between the experiments.

3.2.4 Tidal impacts in the seasonally stratified North Sea

Large parts of the deep northern and central North Sea show a moderate increase in mean annual oceanic CO_2 uptake with tidal forcing (Figure 5D), which indicates that there is a tidal impact

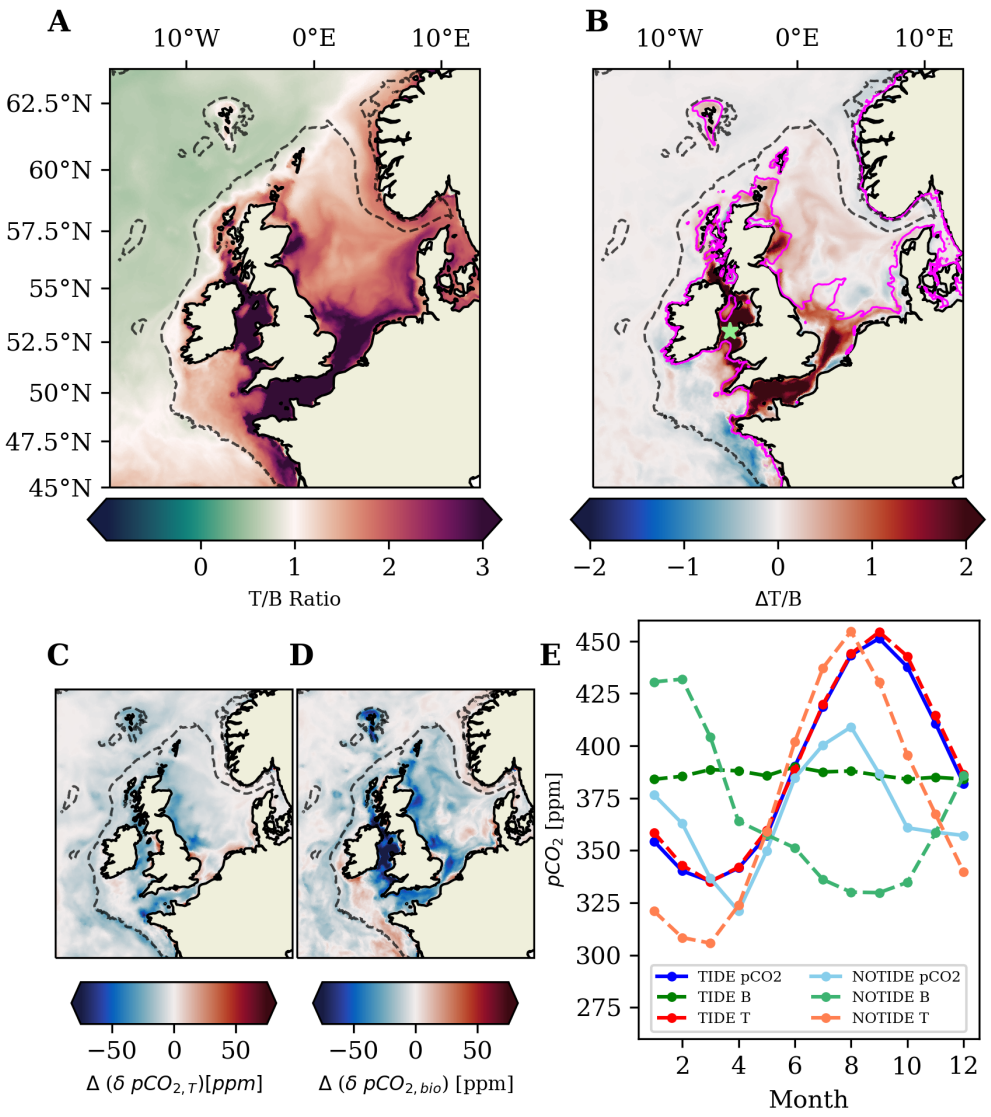

FIGURE 8
(A) T/B ratio of the temperature and biological effects on pCO_2 over the mean annual cycle (2001-2005) in the TIDE experiment calculated with Equation 4. **(B)** Difference in the T/B ratio between the two experiments (TIDE-NOTIDE). Magenta contour indicates PEA= 20 $J\ m^{-3}$ in the TIDE experiment. The difference in the amplitudes of surface pCO_2 changes related to temperature **(C)** and biology **(D)** between the two experiments (TIDE-NOTIDE). **(E)** Surface pCO_2 evaluated at 53°N 5.25°W in the Irish Sea [marked with green star in **(B)**].

specific to these seasonally stratified central and outer-shelf regions. The evaluation of the annual cycle of surface pCO_2 at a station in the northern North Sea shown in Figure 9A demonstrates that the higher annual oceanic CO_2 uptake in the TIDE experiment predominantly stems from lower surface pCO_2 in winter.

We find that the lower winter pCO_2 at the station in the northern North Sea is the result of a weaker biological mitigation of the seasonal cooling effect on pCO_2 in the TIDE experiment (Figure 9A). Heterotrophic remineralization of organic matter produced in summer increases the DIC concentration in the water column in autumn and winter, which constitutes a biological buffering of the effect of seasonal cooling on pCO_2 and controls winter uptake on the shelf. Figure 9C shows that mean winter surface DIC is lower in the TIDE experiment than in the NOTIDE experiment in large parts of the northern and central North Sea, which indicates that the weaker biological mitigation of the seasonal cooling effect on pCO_2 occurs throughout most of the seasonally stratified North Sea.

We find that the difference in the winter DIC concentration in the seasonally stratified North Sea is caused by the tidal impact on benthic-pelagic coupling and associated differences of heterotrophic remineralization between the two experiments (see Sect. 3.2.2). The comparison of the annual cycles of mean DIC in the water column (2001-2005) for the station in the northern North Sea shown in Figure 9E reveals significant tidal impacts on the vertical structure and seasonality of the DIC concentration. In the TIDE experiment, primary production draws down surface layer DIC during the productive season, while vertical POM export and subsequent heterotrophic remineralization increases DIC in the bottom layer (Figure 9D). Resuspension and mixing by strong tidal currents

retains POM in the water column and limits sedimentation. With seasonal cooling at the end of the summer, surface cooling then convectively mixes the DIC-enriched subsurface water to the surface.

Neglecting tides in contrast redistributes heterotrophic remineralization from the water column into the sediment, where heterotrophic remineralization is slower and only diffusively releases DIC into the bottom layer. Bottom layer mixing is also low in the absence of tides, so that the respired DIC accumulates in a shallow bottom boundary layer and leads to substantially higher bottom layer DIC concentrations in the NOTIDE experiment (up to $+30\ mmol\ C\ m^{-3}$; see Figure 9E). The entrainment of the DIC-enriched bottom layer into the water column by December results in higher winter DIC throughout the water column in the NOTIDE experiment, which ultimately leads to higher surface pCO_2 (Figure 9A) and thus lower oceanic CO_2 uptake during winter compared to the TIDE experiment.

Local increases in NCP in the central and northern North Sea with tidal forcing (Figure 7C) imply a reduction of local heterotrophic remineralization relative to local primary production. The local increases in NCP therefore suggest that subsurface advective transport of organic carbon out of the respective shelf areas in the North Sea, predominantly in form of POM (not shown), is more effective in the TIDE experiment than in the NOTIDE experiment. Tidally enhanced advective transport of organic matter in the bottom layer ultimately reduces the magnitude of the biological buffering of the effect of winter cooling on surface pCO_2, and thus contributes to the higher

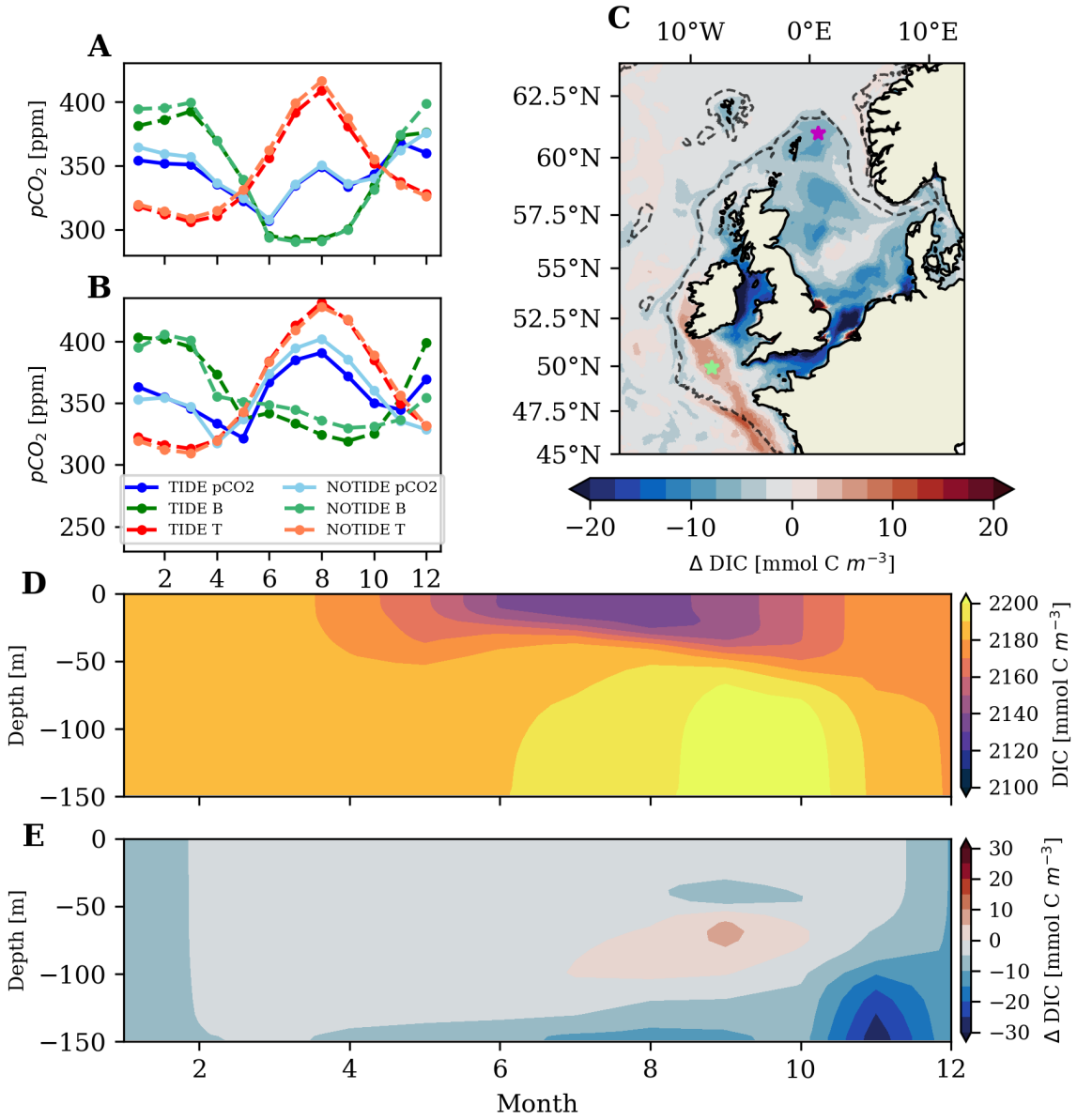

FIGURE 9
Surface pCO_2 evaluated at **(A)** 61°N 0.75°E in the northern North Sea [marked with magenta star in **(C)**] **(B)** 49.9°N 8.2°W in the Celtic Sea (marked with green star in **(C)**. **(C)** Difference in mean surface winter DIC (2001-2005; TIDE-NOTIDE). **(D)** Mean DIC concentration in TIDE experiment and **(E)** difference in mean DIC concentration (TIDE-NOTIDE) at 61°N 0.75°E in the northern North Sea [marked with magenta star in **(C)**].

oceanic CO_2 uptake in winter. We find that about 5% (8.3 *Gmol C* yr^{-1}; Table 2) of the high annual mean oceanic CO_2 uptake in the northern North Sea subarea is related to tides.

3.2.5 Tidal impacts in the seasonally stratified Celtic Sea

Unlike in the North Sea, the majority of the seasonally stratified Celtic Sea shows a decrease in the oceanic CO_2 uptake with tidal forcing (Figure 5D). The evaluation of surface pCO_2 at a station in the central Celtic Sea (Figure 9B) indicates that the dominant cause for the lower annual mean oceanic CO_2 uptake in the TIDE experiment is higher biologically-driven surface pCO_2 in late autumn/early winter. Figure 9C shows corresponding higher winter surface DIC concentrations in the Celtic Sea in the TIDE experiment. The area of higher surface winter DIC in the TIDE experiment extends from the Armorican shelf in the south across the Celtic Sea to the south-west coast of Ireland.

We find a strong tidal impact on the large-scale residual circulation in the Celtic Sea to be the main reason for the difference in winter DIC that causes the regional reduction of oceanic CO_2 uptake with tidal forcing. The seasonal mean depth-averaged residual circulation (2001-2005) and respective seasonal mean surface DIC fields in the TIDE and NOTIDE experiments are documented in Figure 10. Tidal forcing evokes a seasonal cyclonic circulation pattern in the Celtic Sea and Western English Channel not present in the experiment without tides. In summer, Figure 10 shows northward residual transport in the Western English Channel tidal frontal zone and along the south-western UK coast, westward flow at the tidal front in the St. George Channel and a tendency to southeastward flow in the south-western Celtic Sea in the TIDE experiment. Winter (DJF) circulation in the TIDE experiment also shows a tendency to southeastward flow in the south-western Celtic Sea, and weak northwestward flow from the Armorican shelf into the Celtic Sea. The NOTIDE experiment in contrast shows very weak residual circulation in summer. In winter, the NOTIDE experiment shows pronounced northwestward flow from the Armorican shelf across the Celtic Sea. A vertical transect of mean summer horizontal velocity across the south-western Celtic Sea reveals that the cyclonic residual circulation in the TIDE experiment is caused by a near-surface baroclinic current generated at the density gradient of a cold pool trapped below the seasonal thermocline (Figure 11). Such a cold pool flanked by sharp density gradients is only set up in the Celtic Sea with tidal forcing.

The tidal impact on the residual circulation is relevant for air-sea CO_2 exchange because it affects the water mass composition in the Celtic Sea. The strong northward transport in the NOTIDE experiment flushes the Celtic Sea with low-DIC waters from the Armorican shelf and Bay of Biscay in the south, while in the TIDE experiment the Celtic Sea is more influenced by DIC-rich waters from the north, and potentially from the Bristol Channel. Mean winter surface DIC in the Celtic Sea is consequently lower in the NOTIDE experiment than in the TIDE experiment, with the largest difference (up to 20 *mmol C* m^{-3}) occurring in December (not shown). The lower winter DIC concentration in the NOTIDE experiment drives stronger oceanic CO_2 uptake in the Celtic Sea. The seasonally stratified part of the Celtic Sea consequently takes up 49.2 *Gmol C* yr^{-1} more atmospheric CO_2 in the NOTIDE experiment than in the TIDE experiment. This makes up more than 90% of the difference in annual mean oceanic CO_2 uptake between the experiments in the Celtic Sea ($\sim$0.05 *Tmol C* yr^{-1};

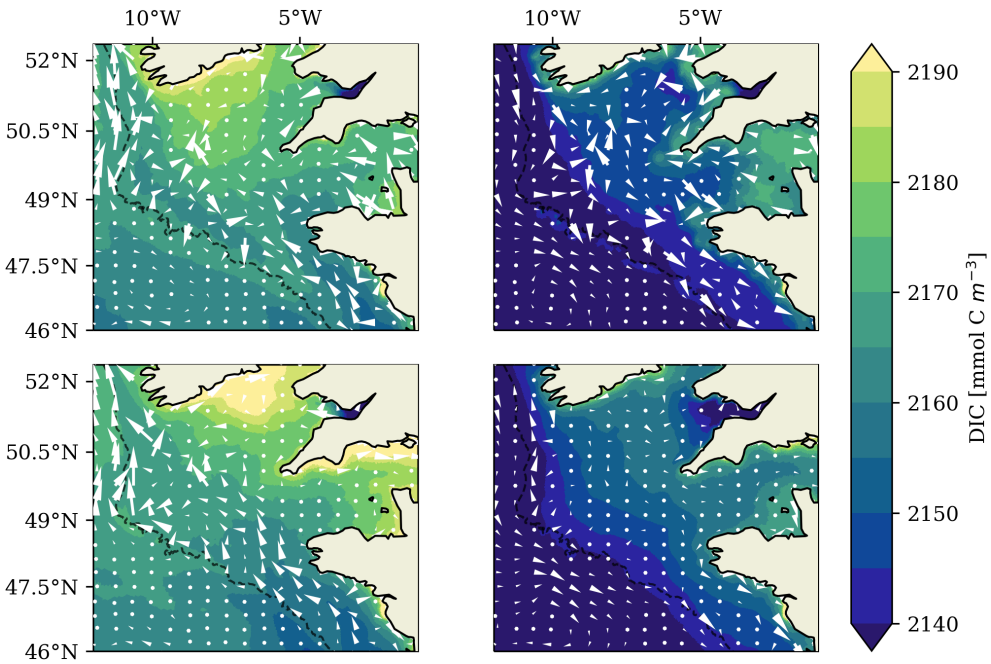

FIGURE 10
Mean winter (left) and summer (right) surface DIC and overlayed seasonal mean depth-averaged residual circulation in the Celtic Sea (2001-2005) in the TIDE experiment (top panel) and NOTIDE experiment (bottom panel).

Table 2), and amounts to ~34% of the difference of the annual mean NWES CO_2 sink between the experiments.

3.2.5.1 Impact of internal tides in the Celtic Sea

The Celtic Sea shelf break and adjacent outer-shelf areas also exhibit a substantial decrease of annual mean oceanic CO_2 uptake with tidal forcing (Figure 5D). The tidal impact at the Celtic Sea shelf break is dominated by internal tides generated by the interaction of tidal flow with the steep local topography. The high-resolution NWES-IT model configuration applied in this study resolves kilometrical-scale internal tides on the NWES (Kossack et al., 2023) and thus allows the investigation of their impact on the shelf carbon cycle. Internal tides produce strong pycnocline mixing at the Celtic Sea shelf break and on the adjacent Celtic Sea shelf, which locally decreases SST and enhances primary production by generating diapycnal nutrient fluxes into the surface layer (New and Pingree, 1990; Sharples et al., 2007; Kossack et al., 2023). We calculate the net effect of pycnocline mixing on surface DIC concentration by computing the difference of the diapycnal DIC flux into the euphotic zone ($J_{DIC}(z_n)$; calculated with Equation 9) and compensatory potential subsurface primary production sustained by the diapycnal nutrient flux into the euphotic zone (calculated with Equation 10). Diapycnal POM and DOM fluxes into the surface layer are found to be negligible.

Figure 12A demonstrates that in the Celtic Sea, the mean summer diapycnal DIC flux into the euphotic zone is marginally overcompensated by primary production sustained by the diapycnal nutrient flux. On the Armorican shelf and in the shallow north-eastern Celtic Sea, the diapycnal DIC flux is larger than the effect of potential new production. The net reduction of surface layer DIC by potential subsurface primary production is mostly < 0.75 $mmol\ C\ d^{-1}$ in the area of tidally enhanced pycnocline mixing along the shelf break of the Celtic Sea. Sites of strong pycnocline mixing at the shelf break or at small-scale bathymetric features on the shelf show a net reduction of surface layer DIC by up to 2 $mmol\ C\ d^{-1}$. Integrated for the south-western Celtic Sea subarea along the shelf break (SWC in Figure 1B), the effect of the dominantly tide-driven pycnocline

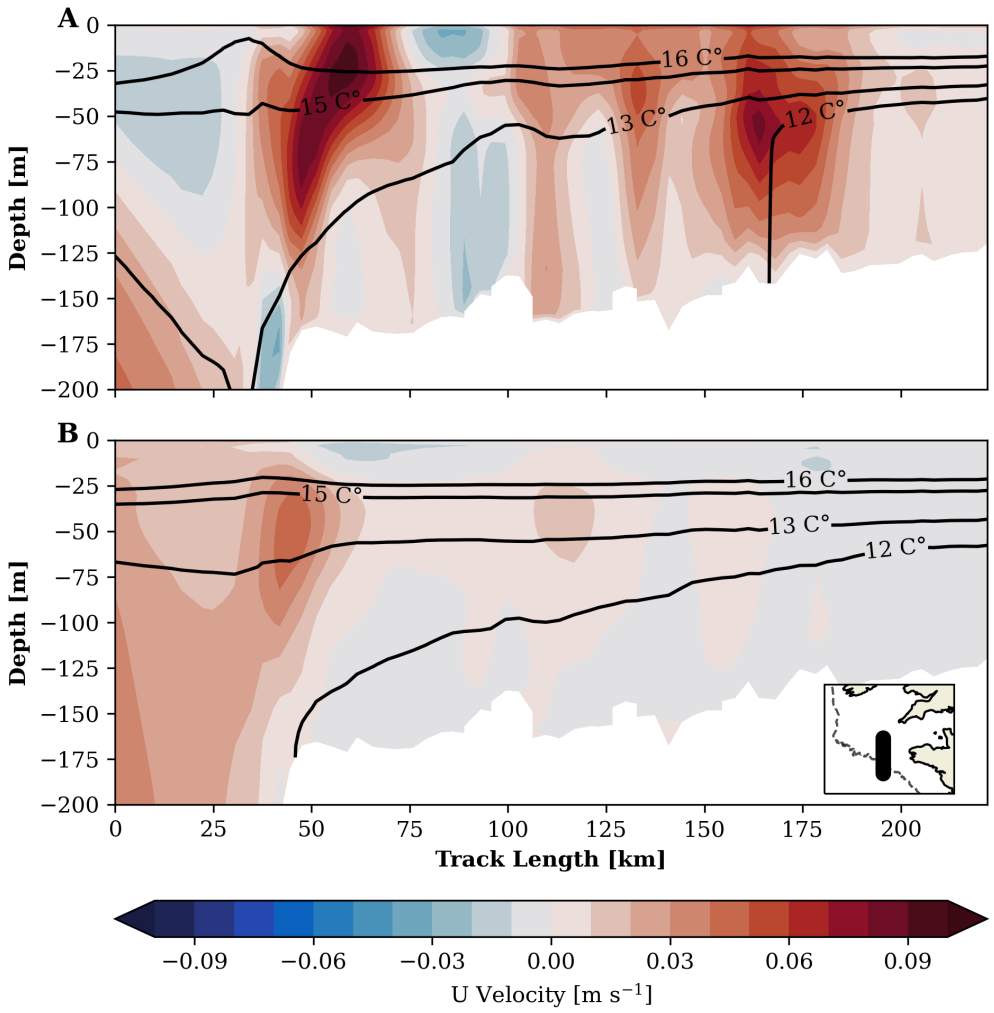

FIGURE 11
Mean summer horizontal u-velocity on transect across Celtic Sea in TIDE experiment **(A)** and NOTIDE experiment **(B)**. Positive values (red) denote eastward flow. Location of transect marked in inset figure in **(B)**.

mixing only amounts to a net reduction of surface layer DIC by -0.8 *Gmol C* over the entire summer (June to August). The low net reduction of surface layer DIC resulting from pycnocline mixing thus only marginally affects the biological control on surface pCO_2 in summer. This is further emphasized by the analysis of surface pCO_2 at a station at the Celtic Sea shelf break in Figure 12B, which only shows a small tidal impact on biological pCO_2 control in summer.

The surface pCO_2 in Figure 12B further illustrates that the tide-driven reduction of local mean annual oceanic CO_2 uptake at the Celtic Sea shelf break rather stems from warmer winter SST and a stronger biological buffering of winter cooling on surface pCO_2 in autumn and winter. The warmer winter SST in the TIDE experiment (see also Supplementary Figure S4B in the Supplementary Material) is likely largely the result of tidally enhanced heat storage in the water column. The relatively stronger biological-driven increase of surface pCO_2 in the TIDE experiment is also evident in the higher winter surface DIC concentrations along the Celtic Sea shelf break (Figure 9C). Our results indicate that the higher surface DIC concentration mainly result from a higher end-of-summer POM concentration in the upper water column above the shelf break in the TIDE experiment (Supplementary Figure S5 in the Supplementary Material). The higher POM concentration results from the overall tidally elevated net primary production at the shelf break (Kossack et al., 2023), but tide-induced turbulent mixing potentially also retains more POM within the reach of the deep winter surface mixed layer.

4 Discussion and conclusion

We use the novel SCHISM-ECOSMO-CO2 model configuration to assess the impact of tidal forcing on oceanic uptake of atmospheric CO_2 on the NWES. Tidal impacts on air-sea CO_2 exchange on the NWES are multifaceted and show high spatial variability. We find tidal forcing responsible for a reduction of mean annual oceanic CO_2 uptake on the NWES by -0.15 *Tmol C* yr^{-1}, which amounts to a ~13% stronger NWES CO_2 sink in the experiment without any tidal forcing.

The dominant tidal impacts on air-sea CO_2 exchange are summarized in Figure 13. Tidal mixing in the permanently mixed shelf regions accounts for the majority (~40%; -0.06 *Tmol C y* r^{-1}) of the tidal weakening of the NWES CO_2 sink. The tidal intensification of temperature control on surface pCO_2 in the permanently mixed shelf regions, and the corresponding decrease in oceanic CO_2 uptake, agrees with prior studies that found tidal mixing to distinctly structure air-sea CO_2 exchange on the NWES

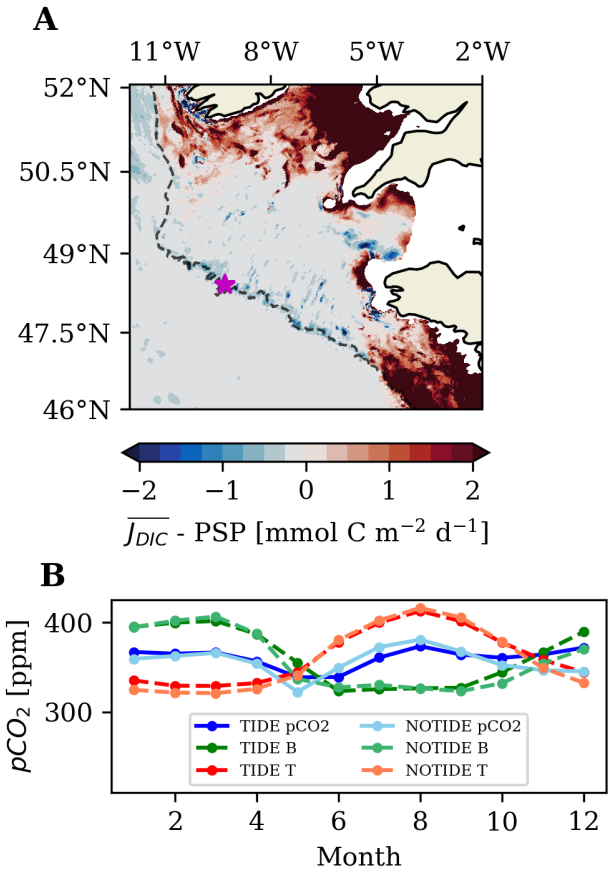

FIGURE 12
Difference of the summer mean turbulent DIC flux (2001-2005; Equation 9) evaluated at the base of the euphotic zone and summer mean potential subsurface primary production (Equation 10) sustained by the turbulent nitrate flux into the surface layer. Permanently mixed regions are masked out. **(B)** Surface pCO_2 evaluated at 14.4°W 53°N on the Celtic Sea shelf break [marked with magenta star in **(A)**].

(Thomas et al., 2004, 2005; Prowe et al., 2009; Omar et al., 2010). Another significant tidal impact on air-sea CO_2 exchange is mediated by the modulation of water mass composition in the Celtic Sea by tide-induced baroclinic circulation, which accounts for ~34% ($-0.05\ Tmol\ C\ yr^{-1}$) of the tidal weakening of the NWES CO_2 sink. Our results indicate that a cyclonic baroclinic circulation induced by a cold and dense bottom pool that is only set up in the presence of tidal forcing contributes to the seasonal near-surface southeastward transport observed in the south-western Celtic Sea (Pingree and Le Cann, 1989; Charria et al., 2013). The presence of cold pools in the Celtic Sea and the importance of associated cyclonic baroclinic circulation was previously suggested in Brown et al. (2003) and Hill et al. (2008). The relevant impact of the tide-induced baroclinic circulation on air-sea CO_2 exchange suggests that projected climate-induced changes of the magnitude of the southeastward flow in the Celtic Sea over the 21st century (Tinker et al., 2024) would likely entail significant local changes in oceanic CO_2 uptake.

The evaluation of net community production in the model describes the NWES as a net heterotrophic system ($NCP = -0.62\ Tmol\ C\ yr^{-1}$). Simulated net heterotrophy of $-0.32\ Tmol\ C\ yr^{-1}$ in the North Sea agrees well with the observational estimate of $-0.3\ Tmol\ C\ yr^{-1}$ provided by Thomas et al. (2005a). We find tidal forcing to strengthen net heterotrophy on the NWES by $-0.04\ Tmol\ C\ yr^{-1}$ (~7% relative to TIDE experiment). Physical resuspension by tides affects the balance of benthic and pelagic heterotrophic remineralization, which in turn modulates the lateral distribution and timing of heterotrophic remineralization on the shelf. Neglecting tides however only results in a minor increase in the net carbon flux to the sediment by POC deposition (by $0.009\ Tmol\ C\ yr^{-1}$), which suggests that the increase in heterotrophy with tides mainly stems from higher organic carbon import onto the NWES. The tidal increase in heterotrophy implies a corresponding decrease in the shelf's uptake capacity for atmospheric CO_2, which contributes the remaining ~26% of the difference in oceanic CO_2 uptake between the experiments. A key finding of this study therefore is that the substantial increase in biological productivity with tidal forcing demonstrated in Kossack et al. (2023) does not translate into a general strengthening of the oceanic CO_2 sink on the shelf.

Our results further suggest that the kilometrical-scale internal tide field does not substantially affect summer-time air-sea CO_2 exchange in the Celtic Sea, in part because of the effective mutual compensation of internal-tide driven diapycnal fluxes of DIC and primary production sustained by diapycnal nutrient fluxes. The identified low impact of diapycnal mixing on air-sea CO_2 exchange in the Celtic Sea is in agreement with Rippeth et al. (2014), who also estimated diapycnal fluxes of nitrate and DIC to largely compensate each other. The hydrostatic model applied in this study likely underestimates pycnocline mixing by the non-hydrostatic internal wave field in the Celtic Sea (Vlasenko et al., 2014). Nevertheless, our results indicate that tide-induced pycnocline mixing impacts the vertical mixing of heat and heterotrophic remineralization on the continental slope of the Celtic Sea. The tidal impacts on the continental slope of the Celtic Sea lead to a substantial local decrease of oceanic CO_2 uptake, which motivates further investigation of internal-tide driven impacts on air-sea CO_2 exchange on the continental slope of the NWES. Our results here suggests that observations of air-sea CO_2 exchange in the area should especially cover the entire seasonal cycle to verify the role of tide-induced pycnocline mixing at the Celtic Sea shelf break.

The presented study considers major bottom-up processes controlling the sensitivity of the shelf carbon cycle to tidal forcing. The 10-m minimum water depths used in this study however limits the representation of very shallow coastal regions, as a wetting and drying scheme is not implemented in the model configuration. The tendency to underestimated oceanic CO_2 uptake on the NWES due to underestimated primary production identified in the model validation (Sect. 2.3) is not expected to significantly affect the sensitivity to tidal forcing, as the tidal response is rather

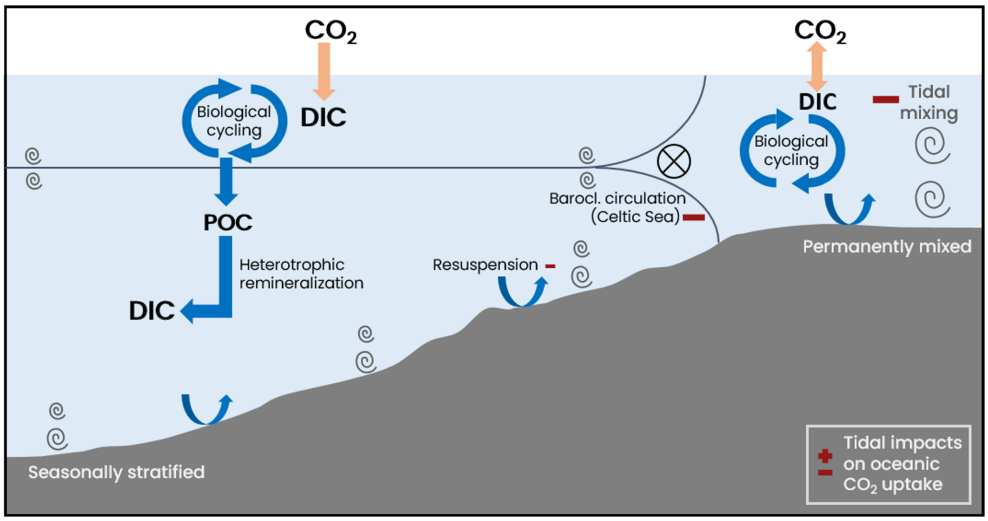

FIGURE 13
Schematic illustration of tidal impacts on air-sea CO_2 exchange on the NWES.

determined by the tidal impact on the balance between net primary production and heterotrophic remineralization. The identified tidal response of the shelf carbon cycle may however be affected by the lack of sediment retention by macrobenthos (Zhang et al., 2019) in the applied model configuration.

The results of this study generally suggest that (subsurface) primary production in seasonally stratified shelf regions sustained by tide-induced pycnocline mixing does not significantly contribute to air-sea CO_2 exchange. As argued in Rippeth et al. (2014), the simulated net sensitivity of the air-sea CO_2 exchange to (tide-induced) pycnocline mixing in summer however relies on the Redfield ratio in phytoplankton growth and is thus limited by the use of constant Redfield stoichiometry in our study. The production and subsequent lateral export of long-lived organic matter with C-rich non-Redfield stoichiometry, as for example shown for the seasonally stratified Celtic Sea by Humphreys et al. (2019), could also marginally increase the sensitivity of oceanic CO_2 uptake to tide-induced pycnocline mixing.

Tidal impacts, mainly the upward transport of respiratory DIC by tidal mixing and the modulation of water mass composition by tide-induced baroclinic circulation in the Celtic Sea, constrain the annual increase of the pelagic DIC stock on the NWES due to the rising atmospheric CO_2 concentration. Neglecting tides therefore results in a higher annual increase of the NWES DIC stock of 0.34 $Tmol\ C\ yr^{-1}$, while the TIDE experiment shows an increase rate of 0.23 $Tmol\ C\ yr^{-1}$. Considering that neglecting tides also increases the carbon flux to the sediment by 0.01 $Tmol\ C\ yr^{-1}$, the difference in the increase rate of the NWES DIC stock (0.11 $Tmol\ C\ yr^{-1}$) implies that only ~20% (0.03 $Tmol\ C\ yr^{-1}$) of the enhanced shelf CO_2 uptake in the experiment without tides (0.15 $Tmol\ C\ yr^{-1}$) is exported off-shelf. Our results therefore suggest that tidal forcing mainly affects carbon reservoirs on the shelf and only marginally modulates off-shelf carbon transport into the North Atlantic. To which extent tidal forcing affects carbon export below the permanent pycnocline critically depends on tidal impacts on the downwelling circulation and cross-shelf fluxes at the shelf break. Tidal impacts on bed stress and friction (Tinker et al., 2022) likely affect Ekman drain in the bottom boundary layer at the shelf break. Previous studies have also demonstrated direct tidal impacts on the European Slope current (Stashchuk et al., 2017; Tinker et al., 2022) that potentially affect the downwelling circulation. Tidal motion further directly affects cross-shelf transports at the shelf break, for example through internal-tide-driven Stokes transport (Spingys et al., 2020; Huthnance et al., 2022). Graham et al. (2018) for example demonstrated relevant on-shelf transport at internal depths likely associated with internal tides on the NWES that is only resolved at kilometrical-scale horizontal model resolution. The evaluation of tidal impacts on cross-shelf fluxes and the downwelling circulation is beyond the scope of this study, but is planned for future work.

In conclusion, our study highlights the importance of representing multifaceted tidal phenomena in ocean models used to investigate marine carbon cycle dynamics on continental shelves. Our simulations at kilometrical-scale horizontal resolution suggest that the effects of tidal mixing, tidal impacts on shelf circulation and benthic-pelagic coupling are most relevant for air-sea CO_2 exchange on the NWES. High-resolution modelling and improved realism of shelf-specific biogeochemical processes has recently been shown to significantly improve coastal carbon dynamics in global ocean models (Mathis et al., 2022) and these improvements in modelling skill further show potential for constraining uncertainties in our understanding of the marine carbon cycle (Mathis et al., 2024). However, as the computational demands likely remain challenging for the near future, further work is required to improve the parameterization of tidal processes in large-scale regional and global model applications.

Data availability statement

The raw data supporting the conclusions of this article will be made available by the authors, without undue reservation.

Author contributions

JK: Data curation, Formal analysis, Investigation, Methodology, Software, Validation, Visualization, Writing – original draft. MM: Conceptualization, Project administration, Resources, Supervision, Writing – review & editing, Methodology. UD: Methodology, Software, Writing – review & editing. FL: Software, Writing – review & editing, Methodology, Validation. KD: Software, Writing – review & editing, Methodology, Validation. HT: Supervision, Writing – review & editing, Validation. CS: Conceptualization, Funding acquisition, Methodology, Project administration, Resources, Supervision, Writing – review & editing, Software.

Funding

The author(s) declare financial support was received for the research, authorship, and/or publication of this article. The research was funded by the Deutsche Forschungsgemeinschaft (DFG, German Research Foundation) under Germany's Excellence Strategy – EXC 2037 'CLICCS - Climate, Climatic Change, and Society' – Project Number: 390683824. The research was also supported by the Helmholtz research program POF IV "The Changing Earth – Sustaining our Future" within "Topic 4: Coastal zones at a time of global change".

Acknowledgments

We would like to thank Yinglong Joseph Zhang for helpful advice regarding the SCHISM model and Nils Christiansen for support with SCHISM configuration and figure design. We would like to thank the reviewers for their time and insights. They have helped improve the manuscript. Computational resources were made available by the German Climate Computing Center (DKRZ) through support from the German Federal Ministry of Education and Research (BMBF). We would like to thank ICDC, CEN, University Hamburg, for data support. This study has been conducted using data from the Global Ocean Data Analysis Project (GLODAP), the Surface Ocean CO2 Atlas

(SOCAT) and the Norwegian Meteorological Institute. The research was funded by the Deutsche Forschungsgemeinschaft (DFG, German Research Foundation) under Germany's Excellence Strategy – EXC 2037 'CLICCS - Climate, Climatic Change, and Society' – Project Number: 390683824 and contributes to the CLICCS subproject A5 – The Land-Ocean Transition Zone. The article processing charges for this open-access publication were covered by the Helmholtz-Zentrum Hereon.

Conflict of interest

The authors declare that the research was conducted in the absence of any commercial or financial relationships that could be construed as a potential conflict of interest.

Publisher's note

Supplementary material

The Supplementary Material for this article can be found online at: https://www.frontiersin.org/articles/10.3389/fmars.2024.1406896/full#supplementary-material

References

Allen, J. I., Holt, J. T., Blackford, J., and Proctor, R. (2007). Error quantification of a high-resolution coupled hydrodynamic-ecosystem coastal-ocean model: Part 2. Chlorophyll-a, nutrients and SPM. *J. Mar. Syst.* 68, 381–404. doi: 10.1016/j.jmarsys.2007.01.005

Arnold, A. K., Lewis, H. W., Hyder, P., Siddorn, J., and O'Dea, E. (2021). The sensitivity of British weather to ocean tides. *Geophys Res. Lett.* 48, e2020GL090732. doi: 10.1029/2020GL090732

Artioli, Y., Blackford, J. C., Butenschön, M., Holt, J. T., Wakelin, S. L., Thomas, H., et al. (2012). The carbonate system in the North Sea: Sensitivity and model validation. *J. Mar. Syst.* 102-104, 1–13. doi: 10.1016/j.jmarsys.2012.04.006

Artioli, Y., Blackford, J. C., Nondal, G., Bellerby, R. G., Wakelin, S. L., Holt, J. T., et al. (2014). Heterogeneity of impacts of high CO2 on the North Western European Shelf. *Biogeosciences* 11, 601–612. doi: 10.5194/bg-11-601-2014

Azam, F., Fenchel, T., Field, J. G., Gray, J. S., Meyer-Reil, L. A., and Thingstad, F. (1983). "The ecological role of water-column microbes in the sea," in *Foundations of Ecology II : Classic Papers with Commentaries*. Eds. T. E. Miller and J. Travis (University of Chicago Press, Chicago), 384–390.

Bakker, D. C. E., Pfeil, B., Landa, C. S., Metzl, N., O'Brien, K. M., Olsen, A., et al. (2016). A multi-decade record of high-quality fCO_2 data in version 3 of the Surface Ocean CO_2 Atlas (SOCAT). *Earth System Sci. Data* 8, 383–413. doi: 10.5194/essd-8-383-2016

Bauer, J. E., Cai, W.-J., Raymond, P. A., Bianchi, T. S., Hopkinson, C. S., and Regnier, P. A. G. (2013). The changing carbon cycle of the coastal ocean. *NATURE* 504, 61–70. doi: 10.1038/nature12857

Becherer, J., Burchard, H., Carpenter, J. R., Graewe, U., and Merckelbach, L. M. (2022). The role of turbulence in fueling the subsurface chlorophyll maximum in tidally dominated shelf seas. *J. Geophys. Res. Oceans* 127, e2022JC018561. doi: 10.1029/2022JC018561

Becker, M., Olsen, A., Landschützer, P., Omar, A., Rehder, G., Rödenbeck, C., et al. (2021). The northern European shelf as an increasing net sink for CO_2. *Biogeosciences* 18, 1127–1147. doi: 10.5194/bg-18-1127-2021

Blackford, J., Artioli, Y., Clark, J., and Mora, L. (2017). Monitoring of offshore geological carbon storage integrity: Implications of natural variability in the marine system and the assessment of anomaly detection criteria. *Int. J. Greenhouse Gas Control* 64, 99–112. doi: 10.1016/j.ijggc.2017.06.020

Blackford, J. C., and Gilbert, F. J. (2007). pH variability and CO2 induced acidification in the North Sea. *Contributions Adv. Mar. Ecosystem Model. Research 27-29 June 2005 Plymouth UK* 64, 229–241. doi: 10.1016/j.jmarsys.2006.03.016

Boyer, T. P., García, H. E., Locarnini, R. A., Zweng, M. M., Mishonov, A. V., Reagan, J. R., et al. (2018). World ocean atlas 2018. Available online at: https://www.ncei.noaa.gov/archive/accession/NCEI-WOA18 (Accessed July 29, 2022).

Bozec, Y., Thomas, H., Schiettecatte, L.-S., Borges, A. V., Elkalay, K., and Baar, H.J.W.d. (2006). Assessment of the processes controlling the seasonal variations of dissolved inorganic carbon in the North Sea. *Limnol. Oceanogr.* 51, 2746–2762. doi: 10.4319/lo.2006.51.6.2746

Brenner, H., Braeckman, U., Le Guitton, M., and Meysman, F. J. R. (2016). The impact of sedimentary alkalinity release on the water column CO_2 system in the North Sea. *Biogeosciences* 13, 841–863. doi: 10.5194/bg-13-841-2016

Broullón, D., Pérez, F. F., Velo, A., Hoppema, M., Olsen, A., Takahashi, T., et al. (2019). A global monthly climatology of total alkalinity: a neural network approach. *Earth System Sci. Data* 11, 1109–1127. doi: 10.5194/essd-11-1109-2019

Broullón, D., Pérez, F. F., Velo, A., Hoppema, M., Olsen, A., Takahashi, T., et al. (2020). A global monthly climatology of oceanic total dissolved inorganic carbon: a neural network approach. *Earth System Sci. Data* 12, 1725–1743. doi: 10.5194/essd-12-1725-2020

Brown, J., Carrillo, L., Fernand, L., Horsburgh, K., Hill, A., Young, E., et al. (2003). Observations of the physical structure and seasonal jet-like circulation of the Celtic Sea and St. George's Channel of the Irish Sea. *Continental Shelf Res.* 23, 533–561. doi: 10.1016/S0278-4343(03)00008-6

Bruggeman, J., and Bolding, K. (2014). A general framework for aquatic biogeochemical models. *Environ. Model. Software* 61, 249–265. doi: 10.1016/j.envsoft.2014.04.002

Charria, G., Lazure, P., Le Cann, B., Serpette, A., Reverdin, G., Louazel, S., et al. (2013). Surface layer circulation derived from Lagrangian drifters in the Bay of Biscay. *XII Int. Symposium Oceanography Bay Biscay* 109-110, S60–S76. doi: 10.1016/j.jmarsys.2011.09.015

Daewel, U., and Schrum, C. (2013). Simulating long-term dynamics of the coupled North Sea and Baltic Sea ecosystem with ECOSMO II: Model description and validation. *J. Mar. Syst.* 119-120, 30–49. doi: 10.1016/j.jmarsys.2013.03.008

Dai, M., Su, J., Zhao, Y., Hofmann, E. E., Cao, Z., Cai, W.-J., et al. (2022). Carbon fluxes in the coastal ocean: synthesis, boundary processes, and future trends. *Annu. Rev. Earth Planet. Sci.* 50, 593–626. doi: 10.1146/annurev-earth-032320-090746

Frankignoulle, M., and Borges, A. V. (2001). European continental shelf as a significant sink for atmospheric carbon dioxide. *Global Biogeochem. Cycles* 15, 569–576. doi: 10.1029/2000GB001307

Graham, J. A., Rosser, J. P., O'Dea, E., and Hewitt, H. T. (2018). Resolving shelf break exchange around the European northwest shelf. *Geophys. Res. Lett.* 45, 12,386–12,395. doi: 10.1029/2018GL079399

Guihou, K., Polton, J., Harle, J., Wakelin, S., O'Dea, E., and Holt, J. (2018). Kilometric scale modeling of the North West European shelf seas: exploring the spatial and temporal variability of internal tides. *J. Geophys. Res. Oceans* 123, 688–707. doi: 10.1002/2017JC012960

Gustafsson, E. (2013). *Modelling the marine CO2 system in BALTSEM* (Stockholm, Sweden: Stockholm University). Available at: https://www.diva-portal.org/smash/get/diva2:1598412/FULLTEXT02.

Hickman, A. E., Moore, C. M., Sharples, J., Lucas, M. I., Tilstone, G. H., Krivtsov, V., et al. (2012). Primary production and nitrate uptake within the seasonal thermocline of a stratified shelf sea. *Mar. Ecol. Prog. Ser.* 463, 39–57. doi: 10.3354/meps09836

Hill, A. E., Brown, J., Fernand, L., Holt, J., Horsburgh, K. J., Proctor, R., et al. (2008). Thermohaline circulation of shallow tidal seas. *Geophys. Res. Lett.* 35. doi: 10.1029/2008GL033459

Hjalmarsson, S., Wesslander, K., Anderson, L. G., Omstedt, A., Perttilä, M., and Mintrop, L. (2008). Distribution, long-term development and mass balance calculation of total alkalinity in the Baltic Sea. *Continental Shelf Res.* 28, 593–601. doi: 10.1016/j.csr.2007.11.010

Holt, J., Harle, J., Wakelin, S., Jardine, J., and Hopkins, J. (2022). Why is seasonal density stratification in shelf seas expected to increase under future climate change? *Geophys Res. Lett.* 49. doi: 10.1029/2022GL100448

Holt, J. T., Allen, J. I., Proctor, R., and Gilbert, F. (2005). Error quantification of a high-resolution coupled hydrodynamic–ecosystem coastal–ocean model: Part 1 model overview and assessment of the hydrodynamics. *Contributions Adv. Mar. Ecosystem Model. Research 27-29 June 2005 Plymouth UK* 57, 167–188. doi: 10.1016/j.jmarsys.2005.04.008

Holt, J., Wakelin, S., Lowe, J., and Tinker, J. (2010). The potential impacts of climate change on the hydrography of the northwest European continental shelf. *Prog. Oceanography* 86, 361–379. doi: 10.1016/j.pocean.2010.05.003

Humphreys, M. P., Achterberg, E. P., Hopkins, J. E., Chowdhury, M. Z., Griffiths, A. M., Hartman, S. E., et al. (2019). Mechanisms for a nutrient-conserving carbon pump in a seasonally stratified, temperate continental shelf sea. *Shelf Sea Biogeochemistry: Pelagic Processes* 177, 101961. doi: 10.1016/j.pocean.2018.05.001

Humphreys, M. P., Schiller, A. J., Sandborn, D., Gregor, L., Pierrot, D., van Heuven, S. M. A. C., et al. (2023). PyCO2SYS: marine carbonate system calculations in Python. *Zenodo*. doi: 10.5281/zenodo.3744275

Huthnance, J., Hopkins, J., Berx, B., Dale, A., Holt, J., Hosegood, P., et al. (2022). Ocean shelf exchange, NW European shelf seas: Measurements, estimates and comparisons. *Prog. Oceanography* 202, 102760. doi: 10.1016/j.pocean.2022.102760

Key, R. M., Olsen, A., van Heuven, S., Lauvset, S. K., Velo, A., Lin, X., et al. (2015). *Global Ocean Data Analysis Project: Version 2 (GLODAPv2). ORNL/CDIAC-162. NDP-093* (Oak Ridge, Tennessee: Carbon Dioxide Information Analysis Center, Oak Ridge National Laboratory, US Department of Energy).

Kitidis, V., Shutler, J. D., Ashton, I., Warren, M., Brown, I., Findlay, H., et al. (2019). Winter weather controls net influx of atmospheric CO2 on the north-west European shelf. *Sci. Rep.* 9, 20153. doi: 10.1038/s41598-019-56363-5

Kossack, J., Mathis, M., Daewel, U., Zhang, Y. J., and Schrum, C. (2023). Barotropic and baroclinic tides increase primary production on the Northwest European Shelf. *Front. IN Mar. Sci.* 10. doi: 10.3389/fmars.2023.1206062

Krumins, V., Gehlen, M., Arndt, S., van Cappellen, P., and Regnier, P. (2013). Dissolved inorganic carbon and alkalinity fluxes from coastal marine sediments: model estimates for different shelf environments and sensitivity to global change. *Biogeosciences* 10, 371–398. doi: 10.5194/bg-10-371-2013

Kühn, W., Pätsch, J., Thomas, H., Borges, A. V., Schiettecatte, L.-S., Bozec, Y., et al. (2010). Nitrogen and carbon cycling in the North Sea and exchange with the North Atlantic—A model study, Part II: Carbon budget and fluxes. *Continental Shelf Res.* 30, 1701–1716. doi: 10.1016/j.csr.2010.07.001

Lan, X., Dlugokencky, E. J., Mund, J. W., Crotwell, A. M., Crotwell, M. J., Moglia, E., et al. (2022). *Atmospheric Carbon Dioxide Dry Air Mole Fractions from the NOAA GML Carbon Cycle Cooperative Global Air Sampling Network 1968-2021: Version: 2022-11-21*. doi: 10.15138/wkgj-f215

Legge, O., Johnson, M., Hicks, N., Jickells, T., Diesing, M., Aldridge, J., et al. (2020). Carbon on the northwest European shelf: contemporary budget and future influences. *Front. IN Mar. Sci.* 7. doi: 10.3389/fmars.2020.00143

Marrec, P., Cariou, T., Macé, E., Morin, P., Salt, L. A., Vernet, M., et al. (2015). Dynamics of air–sea CO_2 fluxes in the northwestern European shelf based on voluntary observing ship and satellite observations. *Biogeosciences* 12, 5371–5391. doi: 10.5194/bg-12-5371-2015

Mathis, M., Elizalde, A., and Mikolajewicz, U. (2018). Which complexity of regional climate system models is essential for downscaling anthropogenic climate change in the Northwest European Shelf? *Clim Dyn* 50, 2637–2659. doi: 10.1007/s00382-017-3761-3

Mathis, M., Lacroix, F., Hagemann, S., Nielsen, D. M., Ilyina, T., and Schrum, C. (2024). Enhanced CO2 uptake of the coastal ocean is dominated by biological carbon fixation. *Nat. Climate Change*. doi: 10.1038/s41558-024-01956-w

Mathis, M., Logemann, K., Maerz, J., Lacroix, F., Hagemann, S., Chegini, F., et al. (2022). Seamless integration of the coastal ocean in global marine carbon cycle modeling. *J. Adv. Model. Earth Syst.* 14 (8), e2021MS002789. doi: 10.1029/2021MS002789

Meyer, M., Pätsch, J., Geyer, B., and Thomas, H. (2018). Revisiting the estimate of the north sea air-sea flux of CO2 in 2001/2002: the dominant role of different wind data products. *J. Geophys. Res. Biogeosci.* 123, 1511–1525. doi: 10.1029/2017JG004281

Millero, F. J., Graham, T. B., Huang, F., Bustos-Serrano, H., and Pierrot, D. (2006). Dissociation constants of carbonic acid in seawater as a function of salinity and temperature. *Mar. Chem.* 100, 80–94. doi: 10.1016/j.marchem.2005.12.001

Neal, C., and Davies, H. (2003). Water quality fluxes for eastern UK rivers entering the North Sea: a summary of information from the Land Ocean Interaction Study (LOIS). *Land Ocean Interaction: processes functioning Environ. management:a UK perspective* 314-316, 821–882. doi: 10.1016/S0048-9697(03)00086-X

New, A. L., and Pingree, R. D. (1990). Evidence for internal tidal mixing near the shelf break in the Bay of Biscay. *Deep Sea Res. Part A. Oceanographic Res. Papers* 37, 1783–1803. doi: 10.1016/0198-0149(90)90078-A

Olsen, A., Key, R. M., van Heuven, S., Lauvset, S. K., Velo, A., Lin, X., et al. (2016). The Global Ocean Data Analysis Project version 2 (GLODAPv2) - an internally consistent data product for the world ocean. *Earth System Sci. Data* 8, 297–323. doi: 10.5194/essd-8-297-2016

Omar, A. M., Olsen, A., Johannessen, T., Hoppema, M., Thomas, H., and Borges, A. V. (2010). Spatiotemporal variations of fCO_2 in the North Sea. *Ocean Sci.* 6, 77–89. doi: 10.5194/os-6-77-2010

Pätsch, J., and Lenhart, H. (2008). Daily loads of nutrients, total alkalinity, dissolved inorganic carbon and dissolved organic carbon of the European continental rivers for the years 1977-2006. *Berichte aus dem Zentrum für Meeres- und Klimaforschung Reihe B: Ozeanographie*. p 48–159.

Pingree, R. D., and Le Cann, B. (1989). Celtic and Armorican slope and shelf residual currents. *Prog. Oceanography* 23, 303–338. doi: 10.1016/0079-6611(89)90003-7

Polton, J. A. (2015). Tidally induced mean flow over bathymetric features: a contemporary challenge for high-resolution wide-area models. *Geophysical Astrophysical Fluid Dynamics* 109, 207–215. doi: 10.1080/03091929.2014.952726

Prowe, A. E. F., Thomas, H., Pätsch, J., Kühn, W., Bozec, Y., Schiettecatte, L.-S., et al. (2009). Mechanisms controlling the air–sea CO2 flux in the North Sea. *Continental Shelf Res.* 29, 1801–1808. doi: 10.1016/j.csr.2009.06.003

Radach, G., and Moll, A. (2006). Review of three-dimensional ecological modeling related to the North Sea shelf system. Part II: Model validation and data needs. In: Gibson, R. N., Atkinson, R. J. A., and Gordon, J. D. M. (Eds.), *Oceanography and marine biology: An annual review*. (CRC Press: Boca Raton). 44, 1–60.

Redfield, A. C., Ketchum, B. H., and Richards, F. A. (1963). The influence of organisms on the composition of seawater. In: Hill, M. N. (Ed.), *The Sea (Vol. 2, The Composition of Sea-Water Comparative and Descriptive Oceanography, pp. 26-77)*, (New York: Interscience Publishers).

Resplandy, L., Hogikyan, A., Müller, J. D., Najjar, R. G., Bange, H. W., Bianchi, D., et al. (2024). A synthesis of global coastal ocean greenhouse gas fluxes. *Global Biogeochem Cycles* 38, e2023GB007803. doi: 10.1029/2023GB007803

Richardson, K., Visser, A. W., and Pedersen, F. B. (2000). Subsurface phytoplankton blooms fuel pelagic production in the North Sea. *J. Plankton Res.* 22, 1663–1671. doi: 10.1093/plankt/22.9.1663

Ricker, M., and Stanev, E. V. (2020). Circulation of the European northwest shelf: a Lagrangian perspective. *Ocean Sci.* 16, 637–655. doi: 10.5194/os-16-637-2020

Rippeth, T. P. (2005). Mixing in seasonally stratified shelf seas: a shifting paradigm. *Philos. Trans. R. Soc. A: Mathematical Phys. Eng. Sci.* 363, 2837–2854. doi: 10.1098/rsta.2005.1662

Rippeth, T. P., and Inall, M. E. (2002). Observations of the internal tide and associated mixing across the Malin Shelf. *J. Geophys. Res.* 107, 928. doi: 10.1029/2000JC000761

Rippeth, T. P., Lincoln, B. J., Kennedy, H. A., Palmer, M. R., Sharples, J., and Williams, C. A. J. (2014). Impact of vertical mixing on sea surface pCO2 in temperate seasonally stratified shelf seas. *J. Geophys. Res. Oceans* 119, 3868–3882. doi: 10.1002/2014JC010089

Rippeth, T. P., Scourse, J. D., Uehara, K., and McKeown, S. (2008). Impact of sea-level rise over the last deglacial transition on the strength of the continental shelf CO 2 pump. *Geophys Res. Lett.* 35. doi: 10.1029/2008GL035880

Sabine, C. L., Hankin, S., Koyuk, H., Bakker, D. C. E., Pfeil, B., Olsen, A., et al. (2013). Surface Ocean CO_2 Atlas (SOCAT) gridded data products. *Earth System Sci. Data* 5, 145–153. doi: 10.5194/essd-5-145-2013

Samuelsen, A., Schrum, C., Yumruktepe, V.Ç., Daewel, U., and Roberts, E. M. (2022). Environmental change at deep-sea sponge habitats over the last half century: A model hindcast study for the age of anthropogenic climate change. *Front. Mar. Sci.* 9. doi: 10.3389/fmars.2022.737164

Schiettecatte, L.-S., Thomas, H., Bozec, Y., and Borges, A. V. (2007). High temporal coverage of carbon dioxide measurements in the Southern Bight of the North Sea. *Special issue: Dedicated to Memory Professor Roland Wollast* 106, 161–173. doi: 10.1016/j.marchem.2007.01.001

Sharples, J. (2008). Potential impacts of the spring-neap tidal cycle on shelf sea primary production. *J. Plankton Res.* 30, 183–197. doi: 10.1093/plankt/fbm088

Sharples, J., Moore, M. C., Rippeth, T. P., Holligan, P. M., Hydes, D. J., Fisher, N. R., et al. (2001). Phytoplankton distribution and survival in the thermocline. *Limnol. Oceanogr.* 46, 486–496. doi: 10.4319/lo.2001.46.3.0486

Sharples, J., Tweddle, J. F., Mattias Green, J. A., Palmer, M. R., Kim, Y.-N., Hickman, A. E., et al. (2007). Spring-neap modulation of internal tide mixing and vertical nitrate fluxes at a shelf edge in summer. *Limnol. Oceanogr.* 52, 1735–1747. doi: 10.4319/lo.2007.52.5.1735

Simpson, J. H., and Hunter, J. R. (1974). Fronts in the Irish sea. *NATURE* 250, 404–406. doi: 10.1038/250404a0

Spingys, C. P., Williams, R. G., Hopkins, J. E., Hall, R. A., Green, J. A. M., and Sharples, J. (2020). Internal tide-driven tracer transport across the continental slope. *J. Geophys. Res. Oceans* 125, e2019JC015530. doi: 10.1029/2019JC015530

Stashchuk, N., Vlasenko, V., Hosegood, P., and Nimmo-Smith, W. A. M. (2017). Tidally induced residual current over the Malin Sea continental slope. *Continental Shelf Res.* 139, 21–34. doi: 10.1016/j.csr.2017.03.010

Takahashi, T., Sutherland, S. C., Sweeney, C., Poisson, A., Metzl, N., Tilbrook, B., et al. (2002). Global sea–air CO2 flux based on climatological surface ocean pCO2, and seasonal biological and temperature effects. *South. Ocean I: Climatic Changes Cycle Carbon South. Ocean* 49, 1601–1622. doi: 10.1016/S0967-0645(02)00003-6

Thomas, H., Bozec, Y., de Baar, H.J.W., Elkalay, K., Frankignoulle, M., Schiettecatte, L.-S., et al. (2005a). The carbon budget of the North Sea. *Biogeosciences* 2, 87–96. doi: 10.5194/bg-2-87-2005

Thomas, H., Bozec, Y., Elkalay, K., and Baar, H.J.W.d. (2004). Enhanced open ocean storage of CO2 from shelf sea pumping. *Science* 304, 1005–1008. doi: 10.1126/science.1095491

Thomas, H., Bozec, Y., Elkalay, K., Baar, H. J. W., Borges, A. V., and Schiettecatte, L.-S. (2005b). Controls of the surface water partial pressure of CO_2 in the North Sea. *Biogeosciences* 2, 323–334. doi: 10.5194/bg-2-323-2005

Thomas, H., Friederike Prowe, A. E., Lima, I. D., Doney, S. C., Wanninkhof, R., Greatbatch, R. J., et al. (2008). Changes in the North Atlantic Oscillation influence CO2 uptake in the North Atlantic over the past 2 decades. *Global Biogeochem. Cycles* 22. doi: 10.1029/2007GB003167

Thomas, H., Schiettecatte, L.-S., Suykens, K., Koné, Y. J. M., Shadwick, E. H., Prowe, A. E. F., et al. (2009). Enhanced ocean carbon storage from anaerobic alkalinity generation in coastal sediments. *Biogeosciences* 6, 267–274. doi: 10.5194/bg-6-267-2009

Tinker, J., Palmer, M. D., Harrison, B. J., O'Dea, E., Sexton, D. M. H., Yamazaki, K., et al. (2024). Twenty-first century marine climate projections for the NW European shelf seas based on a perturbed parameter ensemble. *Ocean Sci.* 20, 835–885. doi: 10.5194/os-20-835-2024

Tinker, J., Polton, J. A., Robins, P. E., Lewis, M. J., and O'Neill, C. K. (2022). The influence of tides on the North West European shelf winter residual circulation. *Front. IN Mar. Sci.* 9. doi: 10.3389/fmars.2022.847138

Tsunogai, S., Watanabe, S., and Sato, T. (1999). Is there a "continental shelf pump" for the absorption of atmospheric CO2? *Tellus B: Chem. Phys. Meteorology* 51, 701–712. doi: 10.3402/tellusb.v51i3.16468

Vlasenko, V., Stashchuk, N., Inall, M. E., and Hopkins, J. E. (2014). Tidal energy conversion in a global hot spot: On the 3-D dynamics of baroclinic tides at the Celtic Sea shelf break. *J. Geophys. Res. Oceans* 119, 3249–3265. doi: 10.1002/2013JC009708

Volk, T., and Hoffert, M. I. (1985). "Ocean carbon pumps: analysis of relative strengths and efficiencies in ocean-driven atmospheric CO2 changes,". In: Sundquist, E. T. (Ed.), *The Carbon Cycle and Atmospheric CO2 : Natural Variations Archean to Present. Geophysical monograph series*. AGU. (Washington, D.C.: American Geophysical Union). 32, 99–110. doi: 10.1029/GM032p0099

Wakelin, S. L., Holt, J. T., Blackford, J. C., Allen, J. I., Butenschön, M., and Artioli, Y. (2012). Modeling the carbon fluxes of the northwest European continental shelf: Validation and budgets. *J. Geophys. Res.* 117, n/a–n/a. doi: 10.1029/2011JC007402

Wang, H., Gong, D., Friedrichs, M. A. M., Harris, C. K., Miles, T., Yu, H.-C., et al. (2022). A cycle of wind-driven canyon upwelling and Downwelling at Wilmington canyon and the evolution of canyon-upwelled dense water on the MAB shelf. *Front. Mar. Sci.* 9. doi: 10.3389/fmars.2022.866075

Wanninkhof, R. (2014). Relationship between wind speed and gas exchange over the ocean revisited. *Limnol. Oceanogr. Methods* 12, 351–362. doi: 10.4319/lom.2014.12.351

Ward, N. D., Megonigal, J. P., Bond-Lamberty, B., Bailey, V. L., Butman, D., Canuel, E. A., et al. (2020). Representing the function and sensitivity of coastal interfaces in Earth system models. *Nat. Commun.* 11, 2458. doi: 10.1038/s41467-020-16236-2

Watson, A. J., Schuster, U., Bakker, D. C. E., Bates, N. R., Corbière, A., González-Dávila, M., et al. (2009). Tracking the variable north Atlantic sink for atmospheric CO2. *Science* 326, 1391–1393. doi: 10.1126/science.1177394

Wolf-Gladrow, D. A., Zeebe, R. E., Klaas, C., Körtzinger, A., and Dickson, A. G. (2007). Total alkalinity: The explicit conservative expression and its application to biogeochemical processes. *Special issue: Dedicated to Memory Professor Roland Wollast* 106, 287–300. doi: 10.1016/j.marchem.2007.01.006

Ye, F., Zhang, Y. J., Yu, H., Sun, W., Moghimi, S., Myers, E., et al. (2020). Simulating storm surge and compound flooding events with a creek-to-ocean model: Importance of baroclinic effects. *Ocean Model.* 145, 101526. doi: 10.1016/j.ocemod.2019.101526

Yu, H.-C., Zhang, Y. J., Yu, J. C., Terng, C., Sun, W., Ye, F., et al. (2017). Simulating multi-scale oceanic processes around Taiwan on unstructured grids. *Ocean Model.* 119, 72–93. doi: 10.1016/j.ocemod.2017.09.007

Zhang, W., Wirtz, K., Daewel, U., Wrede, A., Kröncke, I., Kuhn, G., et al. (2019). The budget of macrobenthic reworked organic carbon: A modeling case study of the North Sea. *J. Geophys. Res. Biogeosci.* 124, 1446–1471. doi: 10.1029/2019JG005109

Zhang, Y. J., Ye, F., Stanev, E. V., and Grashorn, S. (2016). Seamless cross-scale modeling with SCHISM. *Ocean Model.* 102, 64–81. doi: 10.1016/j.ocemod.2016.05.002

Zhao, C., Daewel, U., and Schrum, C. (2019). Tidal impacts on primary production in the North Sea. *Earth System Dynamics* 10, 287–317. doi: 10.5194/esd-10-287-2019